AD NUMBER

AD842594

LIMITATION CHANGES

TO:

Approved for public release; distribution is unlimited.

FROM:

**Distribution authorized to U.S. Gov't. agencies and their contractors;
Administrative/Operational Use; 14 JUN 1960.
Other requests shall be referred to Space and Missile Systems Organization, Los Angeles, CA 90045.**

AUTHORITY

SAMSO ltr 28 Feb 1972

~~SECRET~~ DECLASSIFIED

REPORT NO. AE-60-0496
DATE 6/14/60
NO. OF PAGES 75
Copy No. 35

CONVAIR ASTRONAUTICS
CONVAIR DIVISION OF GENERAL DYNAMICS CORPORATION

CAPABILITY OF ATLAS "F" (C) AS A SPACE VEHICLE BOOSTER

ENGINEERING CORRESPONDENCE
CONVAIR ASTRONAUTICS
POST OFFICE BOX 1128
SAN DIEGO 12, CALIFORNIA
LOG A1246

This document is subject to special export controls and each transmittal to foreign governments or foreign nationals may be made only with prior approval of:
Hq. SAMSO, LA., Ca. 90045
Attn: SMSD

PREPARED BY Preliminary Design and Dynamics Group

CHECKED BY H. B. Steele
H. B. Steele

APPROVED BY K. Kachigan
K. Kachigan

APPROVED BY A. F. Schmitt
A. F. Schmitt

APPROVED BY F. A. Ford
F. A. Ford

APPROVED BY F. J. Dore
F. J. Dore

APPROVED BY H. F. Dunholter
H. F. Dunholter

WS 107A (ATLAS) CLASSIFICATION CHANGED TO:

UNCLASSIFIED

NO.	PAGES AFFECTED

AUTHORIZED BY: AIR FORCE LETTER
SAN BERNARDINO AIR MATERIEL AREA (SBAMA)
DATED 17 NOVEMBER 1965

RECLASSIFIED BY: R J Cook
DEPT. 130-1 DATE 12-13-65

This document ... USC, Sections ... ...ning of the Espionage Laws, Title 18, ...bited by law.

DECLASSIFIED

FORM NO. A-700-3

TABLE OF CONTENTS

LIST OF ILLUSTRATIONS

LIST OF ILLUSTRATIONS (Con't.)

LIST OF TABLES

CAPABILITY OF ATLAS "F" AS A SPACE VEHICLE BOOSTER

1.0 Introduction

The study of the Atlas "F" vehicle has been subdivided into two basic considerations, first as an ICBM and second as a space vehicle booster.

The ICBM is covered by Convair reports:

AE60-0424

AE60-0384

SW-p-17

Missile specifications for missile and ground support.

This report provides results of the study on the Atlas "F" as a space vehicle booster.

2.0 Summary

2.1 This report contains preliminary results of studies conducted on space vehicles made up of the following upper stages, space boosted by an unchanged Atlas "F":

(a) Standard Centaur upper stage,

(b) Growth Centaur upper stage. (Approximately 150% propellant capacity of Standard Centaur),

(c) Standard Centaur used with Centaur Jr. as upper stages. Centaur Jr. is 18000 #gross weight preliminary version.

2.2 Initial studies show that the Atlas "F" vehicle may be used in an unmodified condition as a space booster for each of the three upper stage versions and result in:

(a) Two sigma AMR condition of flight in a completely unmodified condition.

(b) Three sigma operational condition of flight with angle of attack control accomplished by the addition of easily mounted "black box" equipment.

Noteworthy space mission payload results are as follows. More complete results are presented in a later section.

(a) The Atlas "F" with Standard Centaur version has the following payload capability:

(a) 15900# in 100 N.Mile polar orbit.

(b) 3500# in 24 hr. equatorial orbit.

(b) The Atlas "F" with Growth Centaur version has the following payload capability:

(a) 14950# in 100 N. Mile polar orbit.

(b) 4100# in 24 hr. equatorial orbit.

(c) The Atlas "F" with Standard Centaur and Preliminary Centaur Jr. version has the following payload capability:

(a) 4400# in 24 hr. equatorial orbit.

(b) A soft lunar landing of Centaur Jr. with 2200 lb. payload.

3.0 General

The upper stage configurations included in this report may

be used to accomplish a variety of space missions. They are presented in a general manner to show the versatility of each upper stage configuration.

3.1 Configuration descriptions

All three upper stage configurations may be mounted by means of suitable adapters directly to an unmodified Atlas "F".

The Standard Centaur upper stage is an unmodified, presently designed Centaur space vehicle.

The Growth Centaur upper stage maintains all basic Centaur features and components with exception of tank length. Propellant weight capacity is increased to 45000#.

Preliminary
The Centaur Junior upper stage is similar to basic Centaur configuration with the following exceptions:

(a) Gross weight, excluding payload, 18000#.

(b) Tank diameter 8 feet in place of 10 feet.

(c) One 15000# thrust engine instead of two.

3.2 Figure 3.2 shows each upper stage version mounted on the unmodified Atlas "F".

3.3 Configuration weight data is shown in Table 3.3.

3.4 Propulsion data is shown in Table 3.4.

CONVAIR ASTRONAUTICS

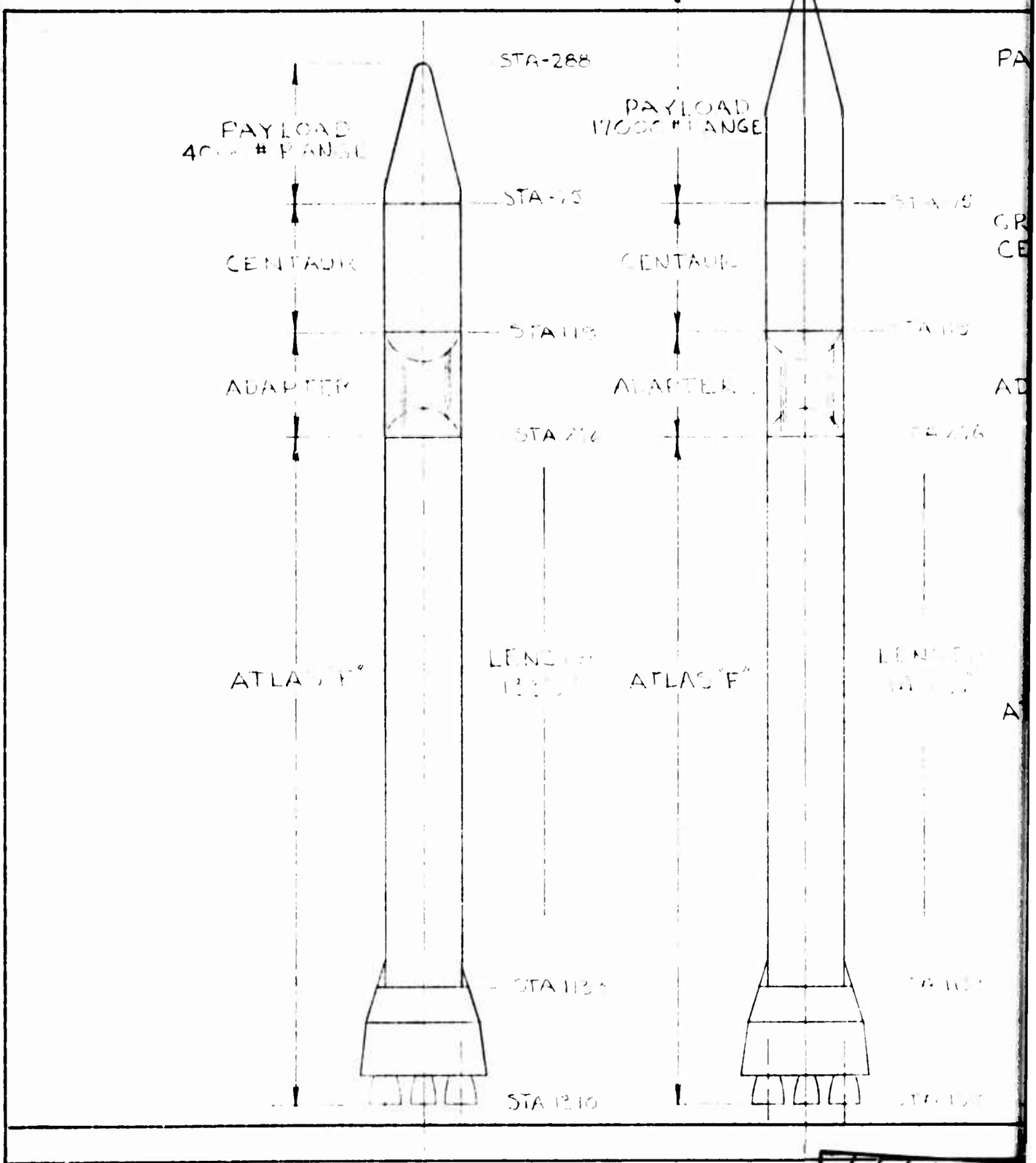

A

FORM NO. A706-4

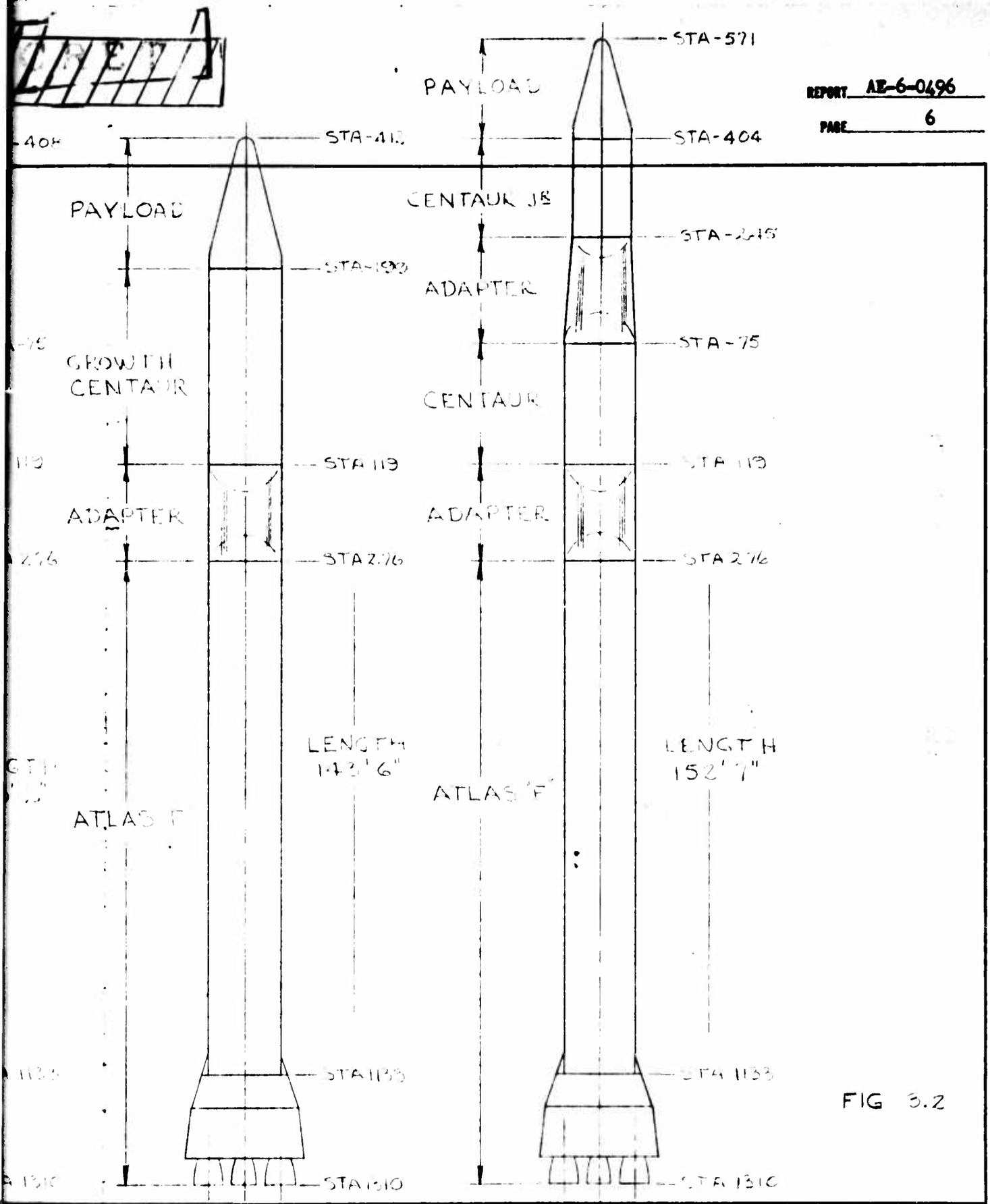

FIG 3.2

PREPARED BY	DATE	CHECKED BY	DATE	REVISED BY	DATE
	5/26/60				

3.5 Loads

3.5.1 Actual maximum bending moments encountered during flight of Standard Centaur space vehicle with Atlas "F" are shown on Figs. 5.14 thru 5.19. Tank B. M. resistance capacity is also shown. It represents bending capacity remaining due to pressure and buckling strength, after axial drag and "g" force loads have been applied. The standard Centaur/Booster configuration has been analyzed in detail. No dynamic work was performed on the growth Centaur or with an upper stage due to lack of time for the study and lack of specific design data on the upper stages.

3.5.2 Atlas "F" tank capacity to resist maximum "g" axial loads is illustrated by Fig. 3.5.2. Booster section burning time before separation has been limited to an amount that will not cause "g" forces to exceed that shown for total weight on Atlas "F". top adapter of each space vehicle considered.

3.5.3 Atlas "F" tank capacity to resist ground wind loads is illustrated by Fig. 3.5.3. Minimum ground tank pressure required per upper stage configuration will be maintained. Weight of Atlas "F" expendable propellants has been adjusted to allow for effect of filling back pressure.

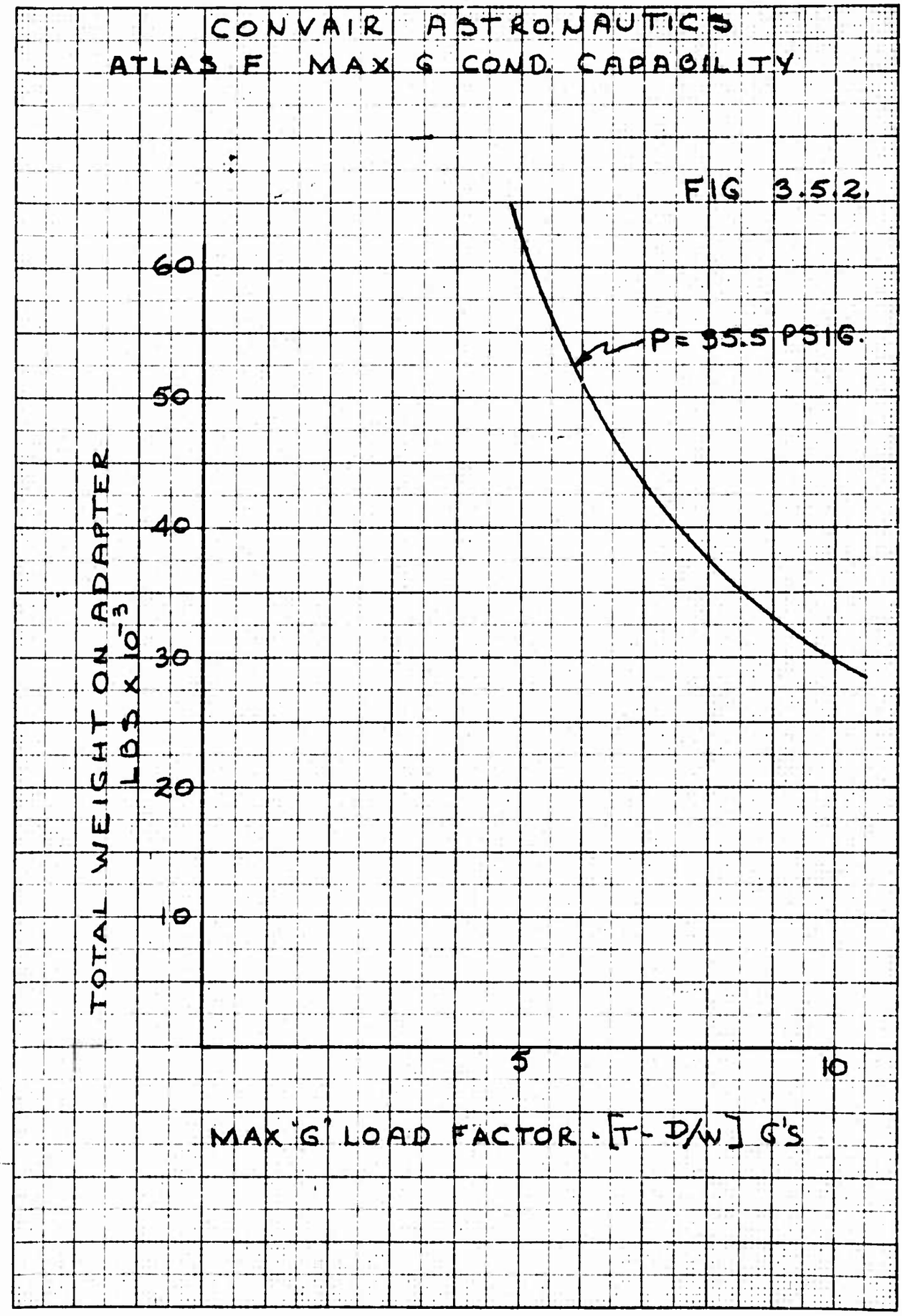

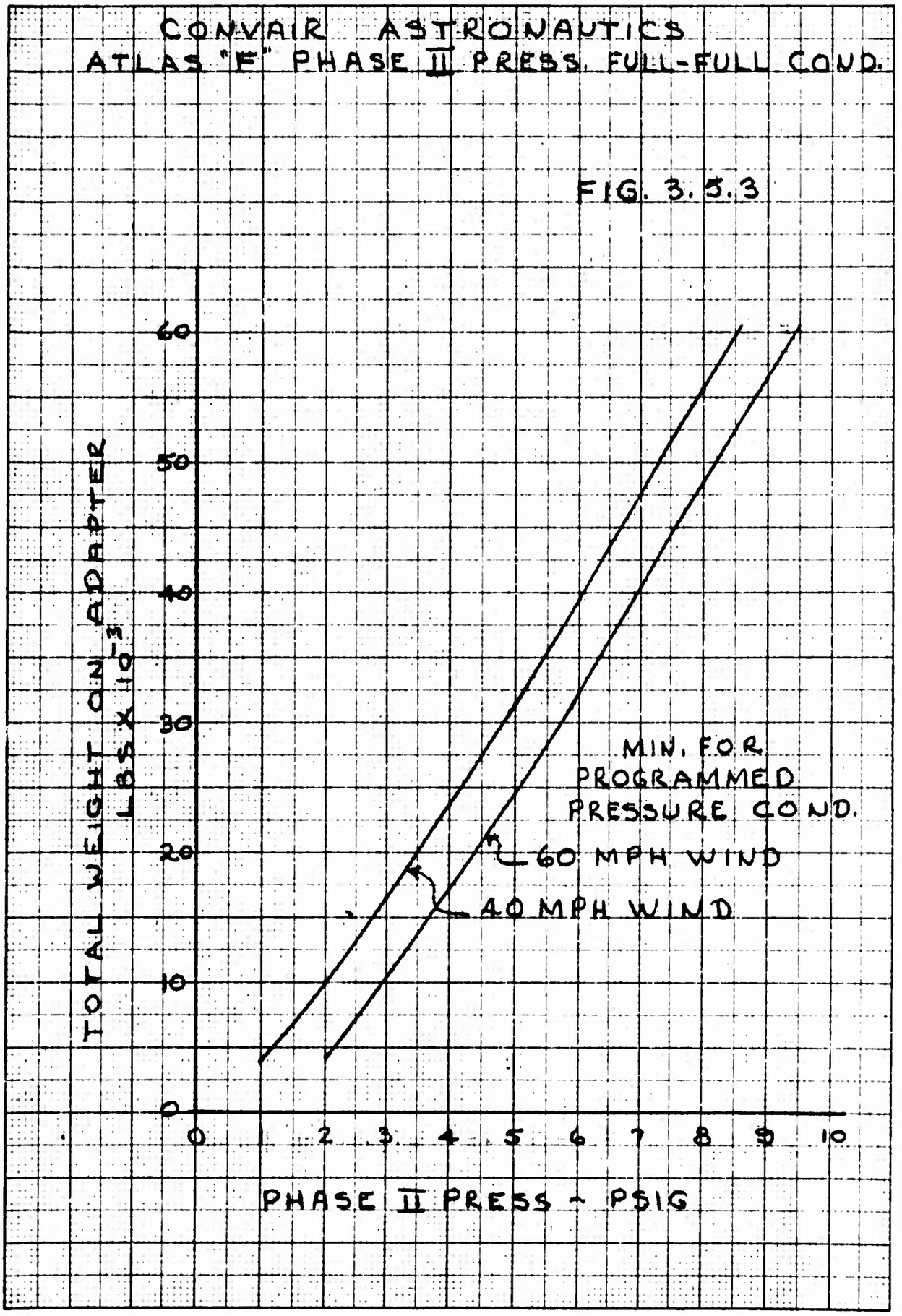

TABLE 3.3 WEIGHT BREAKDOWN

Configuration	Std. Centaur	Std. Centaur	Growth Centaur	Growth Centaur	Std.Centaur Plus Centaur Jr.
Assumed Payload	4000#P.L.	17000# P.L.	5000# P.L.	20000# P.L.	4000 # P.L.
Booster Stage					
Dry Weight (as ICBM)	7051	7051	7051	7051	7051
Residuals	794	794	794	794	794
Low drag fairing	827	827	827	827	662
Upper stage insulation	290	290	435	435	290
	8962	8962	9107	9107	135 8932
Sustainer Stage					
Dry Weight (as ICBM)	6506	6506	6506	6506	6506
Residuals	815	1380	1380	1380	1380
	7321	7886	7886	7886	7886
less frwd. adapter 373					
equip.mtg.&doors 150					
harness in					
adapter 185	708	708	708	708	708
	6613	7178	7178	7178	7178
add Centaur adapter	525	630	630	630	630
Equipment Mtg.	90	90	90	90	90
Range Safety	58	58	58	58	58
	7286	7956	7956	7956	7956
Centaur					
Dry Weight	2794	2794	3685	3685	2794
Residuals	661	661	815	815	661
Centaur Jr. Adapter	3455	3455	4500	4500	410 3865
Centaur Jr.					
Dry Weight					1730
Residuals					270
					2000
Expendables					
Booster Stage	365727	363480	363480	362160	363480
Centaur Stage	29916	29916	45000	45000	29916
Centaur Jr. Stage					16000
Launch Weight	419346	430769	434292	447972	436149

Note: Launch weights shown in this table are based upon assumed Payloads shown.

TABLE 3.4

PROPULSION DATA
(Nominal Thrust and Isp)

Engine	Thrust, lb.		Specific Impulse, sec.	
	Sea Level	Vacuum	Sea Level	Vacuum
Atlas F				
H-2 Booster (2) (E = 12 Pc = 1000)	497020	552238	270.1	300.1
MA-3 Sustainer (E = 25 Pc = 650)	57000	80131	218.4	310.8
Vernier (2) (E = 30 Pc = 500)	900	1200	213.3	284.4
Standard Centaur	--	30000	--	420
Growth Centaur	--	40000	--	428
Centaur Jr.	--	15000	--	420

NOTE: For RP-1 temperature of 60° F and standard conditions outside of the vehicle, the Atlas F propellant densities are: LO_2 = 69.7 lb/ft^3 and RP-1 = 50.4 lb/ft^3. Trajectory calculations made were based upon the influence of propellant density change upon the nominal propulsion data shown in Table 3.4.

4.0 Space Payload Capability

A booster capability study has been conducted to provide performance estimates of the Atlas F using Centaur type upper stages. The standard and growth Centaur 2½ stage configurations were considered as well as a 3½ stage configuration having a Centaur Jr. stage above the standard Centaur.

Calculations of payload capability included the constraints imposed by the axial loading limits of the Atlas F. Figure 4.1 presents the performance of these vehicles in terms of payload at various orbital and space missions. The payloads shown have been degraded to include the effects of boiloff, chilldown flow and restart rockets. Figures 4.2 and 4.3 show the trajectory time history to 100 n.mi. orbital conditions for the standard Centaur configuration with payload for the 24-hour orbit mission. Centaur Jr. propellant loading was optimized for use with the Atlas F and standard Centaur. A soft lunar landing payload of 2200 lbs. was obtained for that configuration.

5.0 Dynamic Analysis

5.1 Summary

A study of dynamic loading, and stability and control has been conducted for the Atlas F plus Centaur vehicles. Details of the study are presented in this section.

Areas of prime importance considered in the investigation are as follows:

A. Dynamic loads

6-16-60
R. J. KONRAD

SPACE CAPABILITY OF ATLAS F WITH CENTAUR TYPE UPPER STAGES

NOTE:
1. NOMINAL PERFORMANCE.
2. AMR LAUNCH.
3. GROWTH CENTAUR WITH LARGE PAYLOADS SHOWS DEGRADED PERFORMANCE DUE TO BOOSTER AXIAL LOAD LIMITING.
4. PAYLOADS INCLUDE EFFECT OF BOIL-OFF, CHILLDOWN & RESTART.

PAYLOAD
X 10^3 LB

DUAL CAST ESCAPE

EQUATORIAL CENTAUR
40,000 LB O_2/H_2
2-20K 420 I_{sp}

POLAR ESCAPE

24 HR EQUATORIAL ESCAPE

STANDARD CENTAUR
29,914 LB O_2/H_2
2-15K 420 I_{sp}

STD. CENTAUR WITH CENT JR.
CENT JR. | 14,000 LB O_2/H_2
1-15K 420 I_{sp}

CENT JR. SOFT LUNAR LAND 22,000 LB PL

VELOCITY ABOVE CIRCULAR AT 100 N.MI. ORBIT X 10^3 FT/SEC

TRAJECTORY TIME HISTORY TO
WITH STANDARD CENTAUR
BOOSTER
Ψ, PSI ~ DEGREES
α, ANGLE OF ATTACK ~ DEGREES
γ, FLIGHT PATH ANGLE ~ DEGREES
q, DYNAMIC PRESSURE ~ LB/FT^2
D, DRAG ~ 1000 LBS
90
80
70
60
50
40
30
20
10
0
-10
-20
-30
800
700
600
500
400
300
200
100
0
52
48
44
40
36
32
28
24
20
16
12
8
4
0
100
D
A
Q
E
γ
Ψ
α

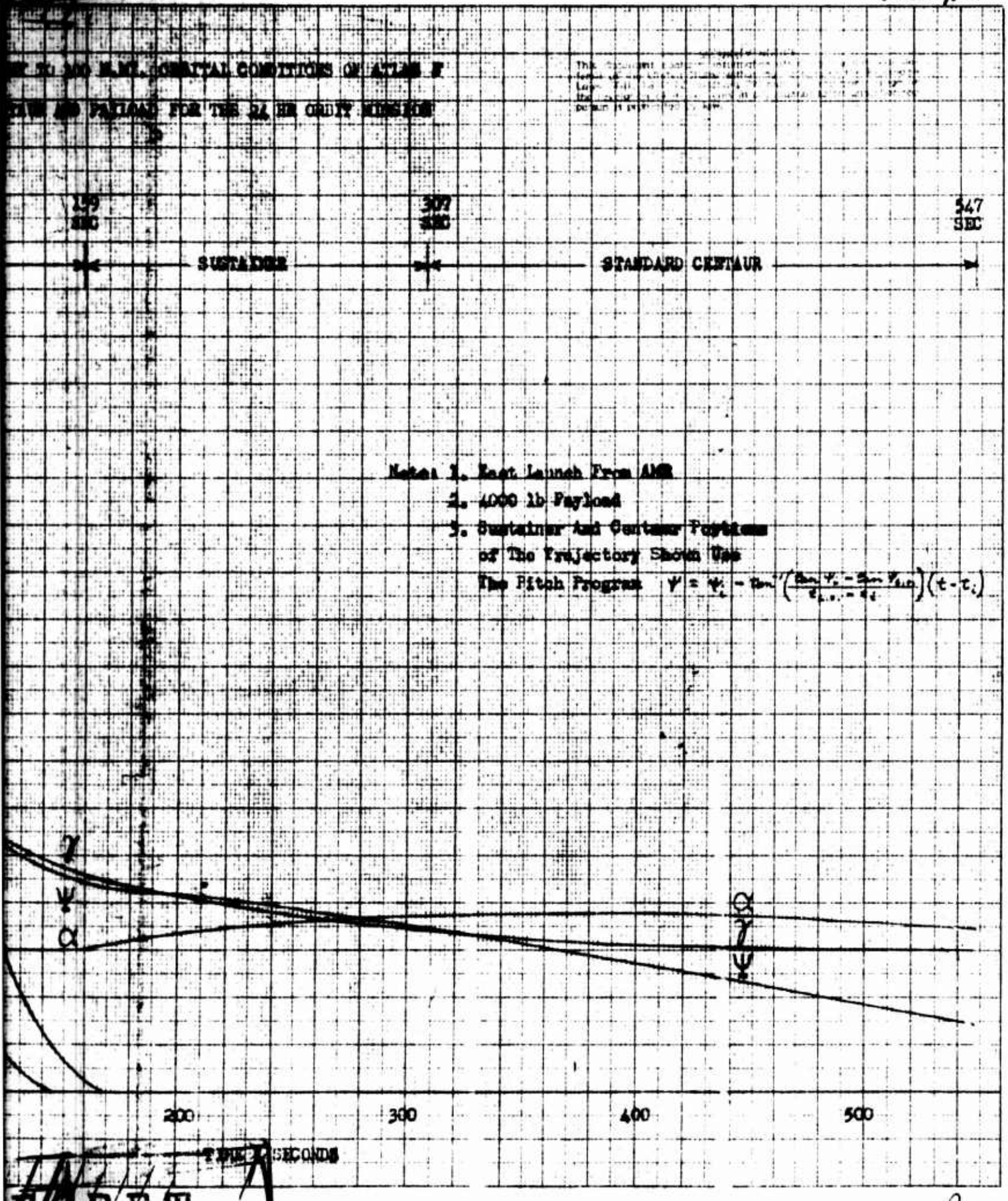
139 SEC
307 SEC
547 SEC
SUSTAINER
STANDARD CENTAUR
Notes 1. East Launch From AMR
2. 4000 lb Payload
3. Sustainer And Centaur Portions
of The Trajectory Shown Use
The Pitch Program
γ
ψ
α
200
300
400
500
TIME - SECONDS

B

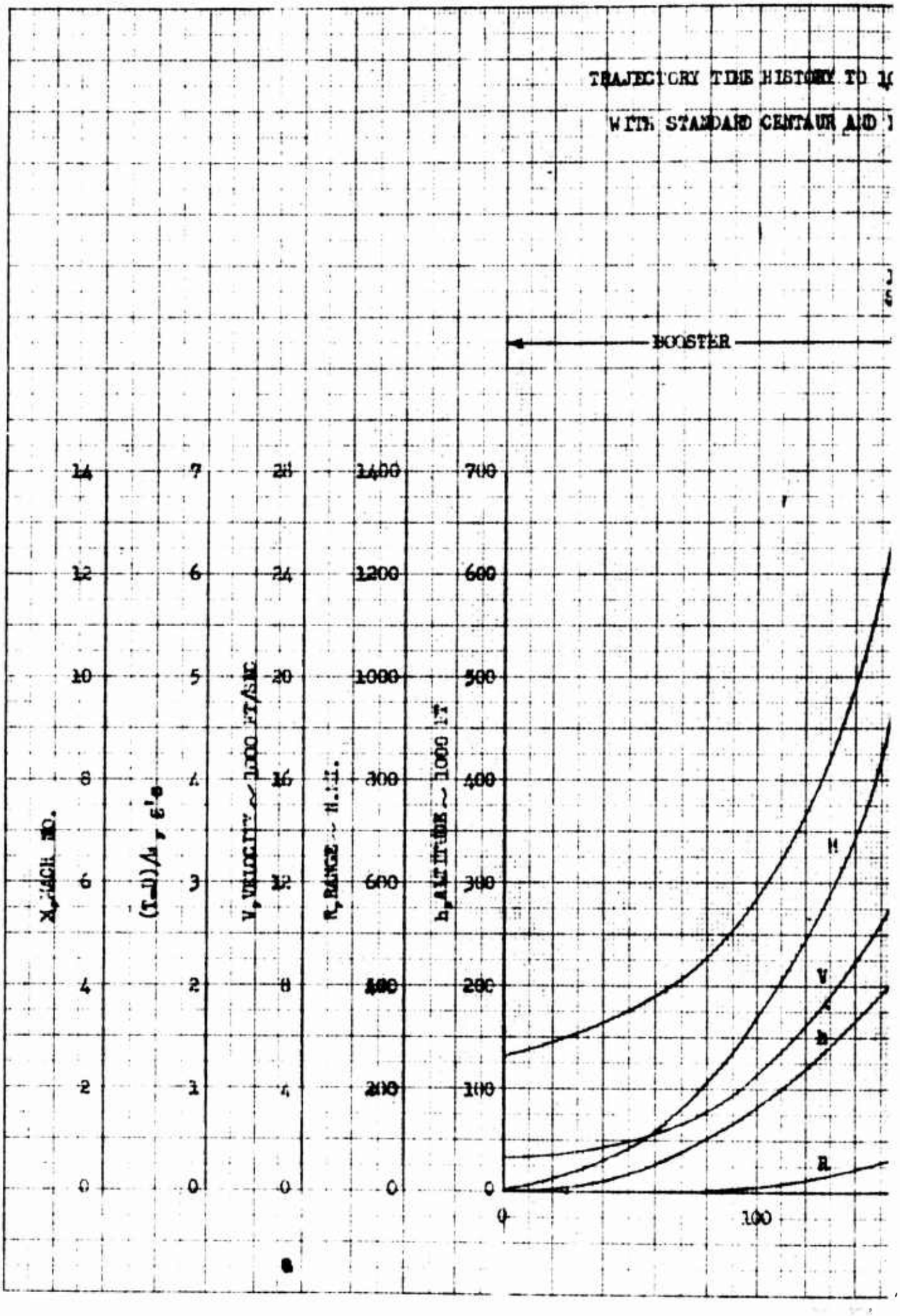
TRAJECTORY TIME HISTORY TO
WITH STANDARD CENTAUR AND
BOOSTER
H
V
h
R
0
100
700
600
500
400
300
200
100
0
1400
1200
1000
800
600
400
200
0
28
24
20
16
12
8
4
0
7
6
5
4
3
2
1
0
14
12
10
8
6
4
2
0

TO 100 N.M. ORBITAL CONDITIONS OF ATLAS F

AND BOOSTER FOR THE 24 HR ORBIT MISSION

152 SEC

307 SEC

547 SEC

SUSTAINER

STANDARD CENTAUR

Notes 1. East Launch From AMR
2. 4000 lb Payload
3. Sustainer And Centaur Portions of The Trajectory Shown Use The Pitch Program $\psi = \psi_{i} - \dot{\psi}_{i}^{-1}\left(\frac{\dot{\psi}_{i}\psi_{i} - \dot{\psi}_{i+1}\psi_{i+1}}{\dot{\psi}_{i} - \dot{\psi}_{i+1}}\right)(t - t_{i})$

T/W

h

V

R

M

(T-D)/W

200

300

400

500

TIME ~ SECONDS

B. Effect of control system augmentation by angle of attack or accelerometer feedback.

C. Sloshing and rigid body stability.

D. Elastic stability.

Two payloads, representative of the mission that the Atlas F plus Centaur vehicle will be called upon to accommodate were considered. These payloads are 4000 pounds and 17000 pounds.

The design values on the Atlas F portion of the vehicle due to longitudinal dynamic loads were those dictated by its application as an ICBM and not attributable to its space booster application.

For the standard control system the bending moments produced by 2 sigma AMR wind conditions are below the limit allowable bending moment, However, by using the standard control system augmented by an angle of attack or accelerometer feedback system the lateral flight loads can be reduced so that they are well below the limit allowable load for all cases considered including the operational wind conditions. Using such auxiliary feedback systems the steady state angle of attack was reduced to .55 degrees and the highest bending moment was decreased from 13.6×10^6 in.-lbs. (for the standard control system) to 6.4×10^6 in.-lbs. (with augmentation) using operational winds.

The results of a time varying analog simulation of the Standard Atlas plus Centaur vehicle employing either angle of

attack or acceleration feedback show that the steady-state angle of attack can be reduced to 0.5 degrees at the time of maximum dynamic pressure. Root loci of these two load alleviation schemes are presented to demonstrate the stability of such methods for the Atlas F plus Centaur vehicle.

Results of analysis of the coupling of the autopilot with the structural bending modes are presented that show that the system is stable through flight. It is shown that coupling of the first bending mode and the Centaur LO_2 tank sloshing at launch when these two modes are at about the same frequency is negligible and should not present a problem. Sloshing stability of the vehicle considering two Atlas F tanks and the Centaur LO_2 tank sloshing is also demonstrated. The propellant sloshing modes were found to be quite stable and suggest reduction of the number of baffles used in the Atlas LO_2 tank.

5.2 Dynamic Loads

5.2.1 Introduction

This section presents the results of an investigation to determine those critical loads that would exist on the Atlas F plus Centaur plus Payload vehicles due to disturbances of a transient or vibratory nature. The investigations put forth are tempered by the fact that the Atlas F portion of the vehicles studied has already undergone an extensive study which is reported in Convair Astronautics Report AE 60-0355, utilizing this vehicle as an ICBM booster. In order to effect some consistency in the treatment of dynamic loading the design conditions put forth in Report AE 60-0355 will be applied to the Atlas F plus Centaur plus Payload combinations and comparisons of the derived dynamic loads effected. Where this treatment produced design loads in excess of those rendered by the treatment of the Atlas F as an ICBM carrier, practical load relieving mechanisms are considered. These mechanisms are discussed with practical application and high reliability as a guide to their use. This dual study is being undertaken in order to determine the practicability of using an unmodified Atlas F vehicle (which was designed by ICBM considerations) as a booster for various upper stages.

The upper stages considered in this study were Centaur with a 4000 pound payload and Centaur with a 17000 pound payload.

5.2.2 Ground Wind Loading (Including Effects of Random Vortex Shedding

When the Atlas F plus Centaur missile is erected and exposed on the ground it must be capable of resisting the loads produced by the application of ground winds. The intensity of the impinging wind will be a function of the site selected for launch, of this vehicle and the design risk for this condition which is commensurate with the mission philosophy. For the purposes of the study two values of equivalent steady wind intensities were assumed, namely:

1. A 40 mph equivalent steady wind velocity which value is exceeded only .3% of the time, on the average, at the Atlantic Missile Range (AMR). This value is referred to as a 3 sigma value at AMR.
2. A 60 mph equivalent steady wind velocity which value is exceeded only 1% of the time, on the average, over the continental United States. This value is referred to as the Operational 1% Risk Value.

When the design loading conditions were formulated for the ground winds recognition of not only the effects produced by steady winds were accounted for but also of the effects produced by vortices being shed by the vehicle. The problem or random vortex shedding of the winds around a cylinder have been the

subject of recent studies by the NASA Ames Staff and Dr. Y. C. Fung of S.T.L. These studies have shown that in the supercritical Reynolds Number region (which occurs on the Atlas F plus Centaur vehicles when exposed to both 40 mph and 60 mph winds) random vortices will be shed by the vehicle in both the lift and drag planes. These vortices, although random in nature, possess sufficient strength at the lower frequencies to excite the missiles cantilever modes which produces loads in excess of those predicted by two-dimensional steady state aerodynamic theory. It is, therefore, imperative for the design of this vehicle that these effects be included where applicable.

In order to predict the loads which would be imposed on the erected, exposed Atlas F plus Centaur missile combinations the power spectral inputs used were those after the study of Fung, utilizing an auto-correlation coefficient of 1 to express the random vortex distribution along the vehicle length. A steady drag coefficient, C_D, of .0.525 was used for both the 40 mph and 60 mph wind cases. Also, since the strength of the random vortices shed increases with lower frequency, all stages of the missile were assumed to be fully tanked with a 17,000 lb. payload atop the Centaur. This condition provided the lowest missile cantilever frequency and resulted in the highest vortex shedding loads. The bending moments produced by the steady drag, oscillatory

lift forces on the missile were combined vectorially to render a resultant bending moment distribution along the length of the missile. This distribution is shown in Figure 5.1 for both the 40 mph and 60 mph wind cases. In order to determine the total bending moment distribution along the missile the effects of misalignments, disconnect forces, etc. should be combined with this value.

When the vehicle is in a condition of tanking where less than the full amounts of liquids are aboard the bending moments produced by ground winds, including the effects of random vortex shedding, will be less than those shown in Figure 5.1.

5.2.3 Longitudinal Dynamics Loads

When the Atlas F plus Centaur vehicle is subjected to the rapidly varying engine thrust forces produced by booster and sustainer build-up and cut-off, longitudinal dynamic loads are imposed on the vehicle structure. In order to ascertain the magnitude of these dynamic loads a spring-mass model, representing the mass and stiffness characteristics of the vehicle together with those lateral distortions of the tank structure produced by an accelerating columnof liquid, will be subjected to these engines thrust build-up and cut-off characteristics.

These engine characteristics were obtained from NAA and are

5.1

FIGURE

ATLAS F PLUS CENTAUR WITH A 4000 LB PAYLOAD
BENDING MOMENTS DUE TO GROUND WIND INCIDENCE
THE EFFECTS OF RANDOM TURBULENCE

NOTE: ALL PROPELLANT TANKS FULL
FUNG DATA
NO MISALIGNMENTS OR SECONDARY
EFFECTS INCLUDED

ATLAS F + CENTAUR
V_w = 60 MPH

ATLAS F + CENTAUR
V_w = 40 MPH

BENDING MOMENT ~ INCH-POUNDS X 10^{-6}

MISSILE STATION ~ INCHES

PREPARED BY	DATE	CHECKED BY	DATE	REVISED BY	DATE
K. Leadley	5-23-60				

their best conservative estimate of these parameters at this time. A typical booster and sustainer engine thrust build-up curve is shown in Figure 5.2 The delay time between booster and sustainer thrust build-up is intentional in order to diminish the loading felt by the vehicle structure. This value is the same as was used on the SM-65E missiles.

The missile was examined for captive thrust build-up and free launch at both sea level and altitude (10,000 feet).

The maximum accelerations experienced by the LO_2 and Fuel liquids (which are of prime concern in tank design) for both captive and thrust build-up and free launch are shown in Table 5.1. Also shown are those accelerations which would be imposed on the Atlas F LO_2 and Fuel liquids when this vehicle is used as an ICBM. It should be noted that for a dual capability design on the Atlas F booster the design loading conditions are due to use of the vehicle as an ICBM. Therefore, for these conditions the space applications of the Atlas F are not designing conditions.

The maximum acceleration experienced by the LO_2 and Fuel liquids due to captive thrust cut-off were also derived. It was assumed that the engine thrust forces would decay from 100% to 10% thrust values in 0.2 seconds, simultaneously for all engines. These values are shown in Table 5.1 Also shown are comparable values on the Atlas F when used as an ICBM. Here again comparison of the

FIGURE 5.2

ATLAS F SERIES MISSILE

ESTIMATED THRUST BUILD UP CHARACTERISTICS

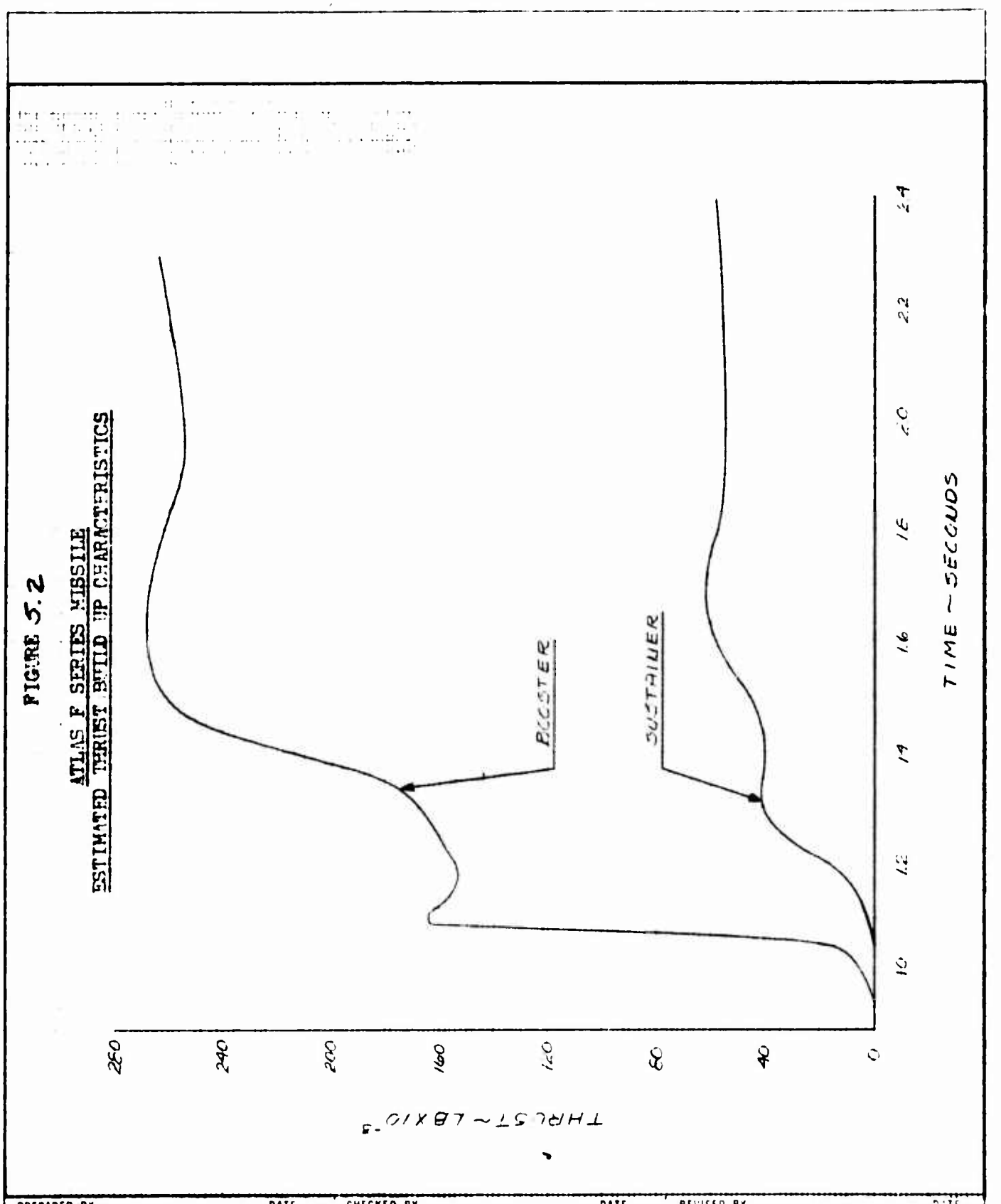

PREPARED BY	DATE	CHECKED BY	DATE	REVISED BY	DATE
JJ Acree	3-23-60				

THRUST BUILD-UP AND CUT-OFF LOAD FACTORS ON THE ATLAS F LIQUIDS FOR VARIOUS UPPER STAGE LOADS

MISSILE CONF.	LAUNCH ALTITUDE	LONG. LIMIT DESIGN LOAD FACTORS					
		CAPTIVE THRUST B.U.		CAPTIVE THRUST C.O.		FREE LAUNCH	
		η_F	η_L	η_F	η_L	η_F	η_L
Atlas F ICBM	Sea Level	2.5g	1.15g	1.23g	2.13g	2.13g	1.66g
	10,000'	2.6g	1.16g	1.25g	1.25g	2.22g	1.75g
Atlas F + Centaur + 4000# P/L	Sea Level	2.5g	1.15g	1.23g	1.23g	2.04g	1.57g
	10,000'	2.6g	1.16g	1.25g	1.25g	2.13g	1.66g
Atlas F + Centaur + 17,000# P/L	Sea Level	2.5g	1.15g	1.23g	1.23g	2.02g	1.55g
	10,000'	2.6g	1.16g	1.25g	1.25g	2.10g	1.63g

η_F = Limit longitudinal load factor on Atlas F fuel liquid

η_L = Limit longitudinal load factor on Atlas F LO_2 liquid

TABLE 5-1

accelerations show that the design loading conditions are due to the use of the vehicle as an ICBM.

In-flight booster engine cut-off was again assumed to take 0.2 seconds to decay from 100% to 10% of booster thrust and produced very small accelerations on the liquid. The same is true of in-flight sustainer cut-off.

In summary it is shown that the design values on the Atlas F portion of this vehicle combination are those produced by its application as an ICBM and not attributable to its space booster application.

5.2.4 Vibration Characteristics of the Vehicle

It is convenient in calculating the flight loads and stability characteristics on the flexible-bodied vehicle to express its elastic properties in terms of free-free natural frequencies and mode functions. Using normal mode theory, the stability and loads analyses are easily performed. Vibration characteristics of the Atlas F plus Centaur with both a 4000 pound and a 17,000 pound payload were determined using a lumped mass distribution of 33 stations and an influence coefficient matrix for 32 stations. Influence coefficients were developed from calculated beam bending and shear stiffness data.

The calculations were performed for three time instants during the boost phase of flight, namely:

1. Missile fully tanked (t = 0)

2. Missile at time of maximum dynamic pressure (t = 60 sec.)

3. Missile at time prior to booster engine cut-off (t = 128 sec.)

In all cases any significant sloshing masses were removed. These masses were coupled back into the overall dynamic equations of motion as generalized forces for the time dependent solutions.

The natural frequencies and generalized masses for the first five elastic modes of vibration are summarized in Table 5.2 Also presented are the corresponding parameters for the Atlas F missile when used as an ICBM.

Plots of the deflected shapes of the first three elastic modes of vibration for both payloads at t = 0, t = 60 sec., and t = 128 seconds are shown in Figures 5.3 through 5.8

Plots of the node point variations of the first three modes with time for the two vehicles are shown in Figures 5.9 and 5.10 Also plotted in Figure 5.11 are the corresponding nodal variations for the Atlas F when used as an ICBM.

5.2.5 Lateral Flight Loads

In approaching the problem of determining the lateral flight loads on the Atlas F plus Centaur plus Payload vehicle two studies were performed, namely:

1. Lateral flight loads imposed by using a standard control system similar to that used on the Atlas F ICBM (i.e.

MISSILE	ω_1 rad/sec	m_1 slugs	ω_2 rad/sec	m_2 slugs	ω_3 rad/sec	m_3 slugs	ω_4 rad/sec	m_4 slugs	ω_5 rad/sec	m_5 slugs
Atlas F										
t = 0	11.63	3882	25.67	5844	43.63	5230	63.62	4481	84.29	7151
t = 60	12.57	5082	35.25	4770	71.00	2003	96.51	5057	140.56	35826
t = 128	14.80	2359	99.97	5151	150.70	2562	162.90	5694	232.00	246,374
F+Centaur 4,000 P/L										
t = 0	10.57	4162	23.42	5553	41.34	5537	58.30	6315	71.61	6857
t = 60	10.82	4348	33.35	5330	51.43	15486	72.66	2045	98.30	6465
t = 128	13.74	2099	43.82	45338	106.84	4587	160.21	12360	-	-
F+Centaur 17000 P/L										
t = 0	7.34	4967	17.87	5014	32.95	6784	49.09	5583	67.57	4811
t = 60	7.86	3738	22.65	10552	39.05	5659	72.03	1991	97.85	6238
t = 128	10.75	2109	23.45	8910	105.45	4769	132.38	44538	156.45	1927

NATURAL MODAL FREQUENCIES AND MASSES
ATLAS F PLUS SPACE SERIES

TABLE 5.2

5.3

FIGURE 5.3

ATLAS F CENTAUR WITH A 4000 LB PAYLOAD
DEFLECTION VS. STATION FOR THE FIRST THREE NATURAL MODES OF VIBRATION AT LAUNCH

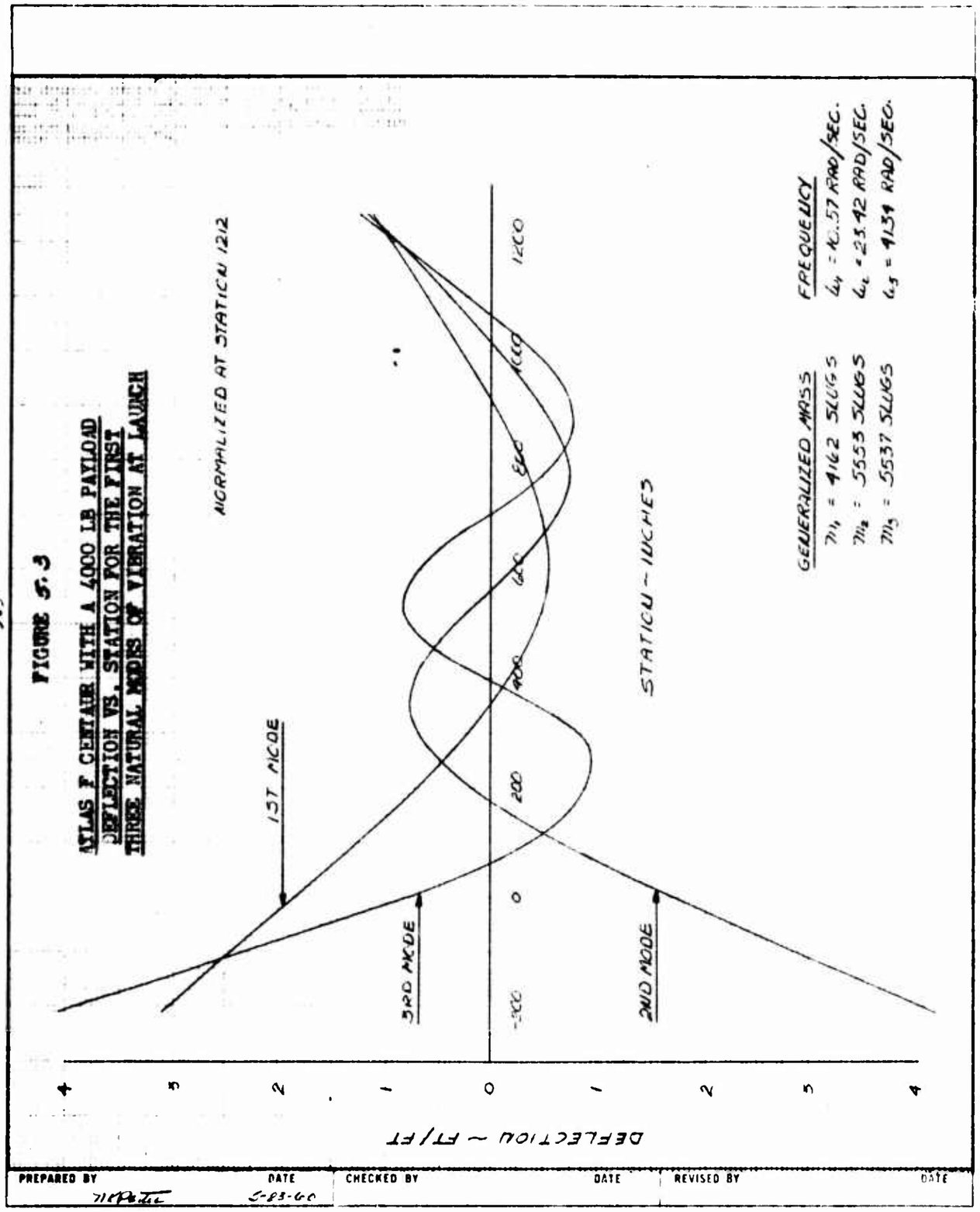

PREPARED BY	DATE	CHECKED BY	DATE	REVISED BY	DATE
[illegible]	5-23-60				

FORM NO. A1107-1

5.4

FIGURE 5-4

ATLAS 'D' CENTAUR WITH A 4000 LB PAYLOAD
DEFLECTION VS. STATION FOR THE FIRST
THREE NATURAL MODES OF VIBRATION AT
TIME OF MAXIMUM DYNAMIC PRESSURE

NORMALIZED AT STATION 1212

GENERALIZED MASS	FREQUENCY
M_1 = 4348 SLUGS	ω_1 = 10.82 RAD/SEC
M_2 = 5330 SLUGS	ω_2 = 3335 RAD/SEC.
M_3 = 15466 SLUGS	ω_3 = 5145 RAD/SEC.

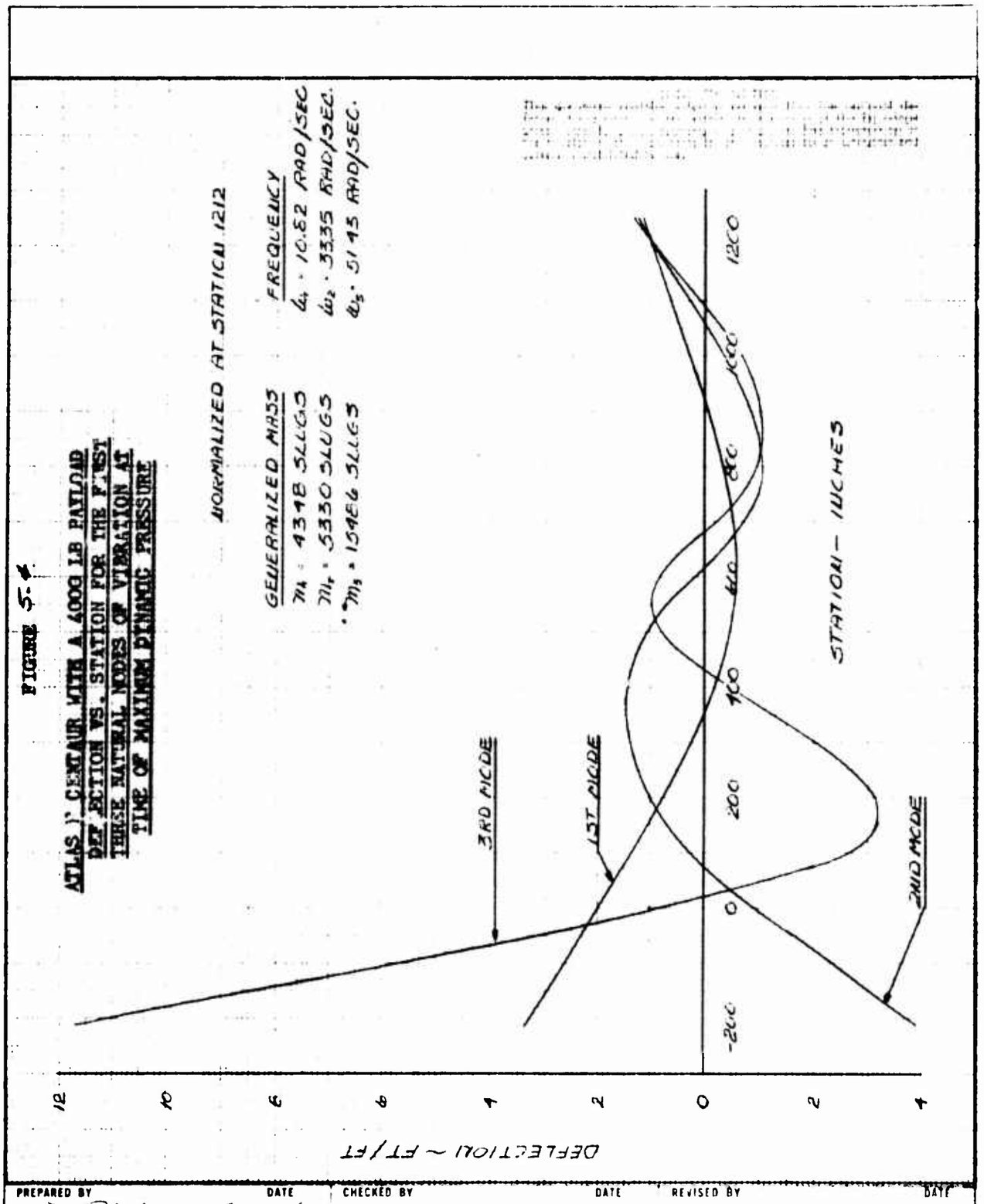

PREPARED BY	DATE	CHECKED BY	DATE	REVISED BY	DATE
J. Dietz	5-23-60				

FORM NO. A1107-1

5.5

FIGURE 5.5

ATLAS F PLUS CENTAUR WITH A 4000 LB PAYLOAD
DEFLECTION VS. STATION FOR THE FIRST THREE
NATURAL MODES OF VIBRATION JUST
PRIOR TO BOOSTER CUTOFF

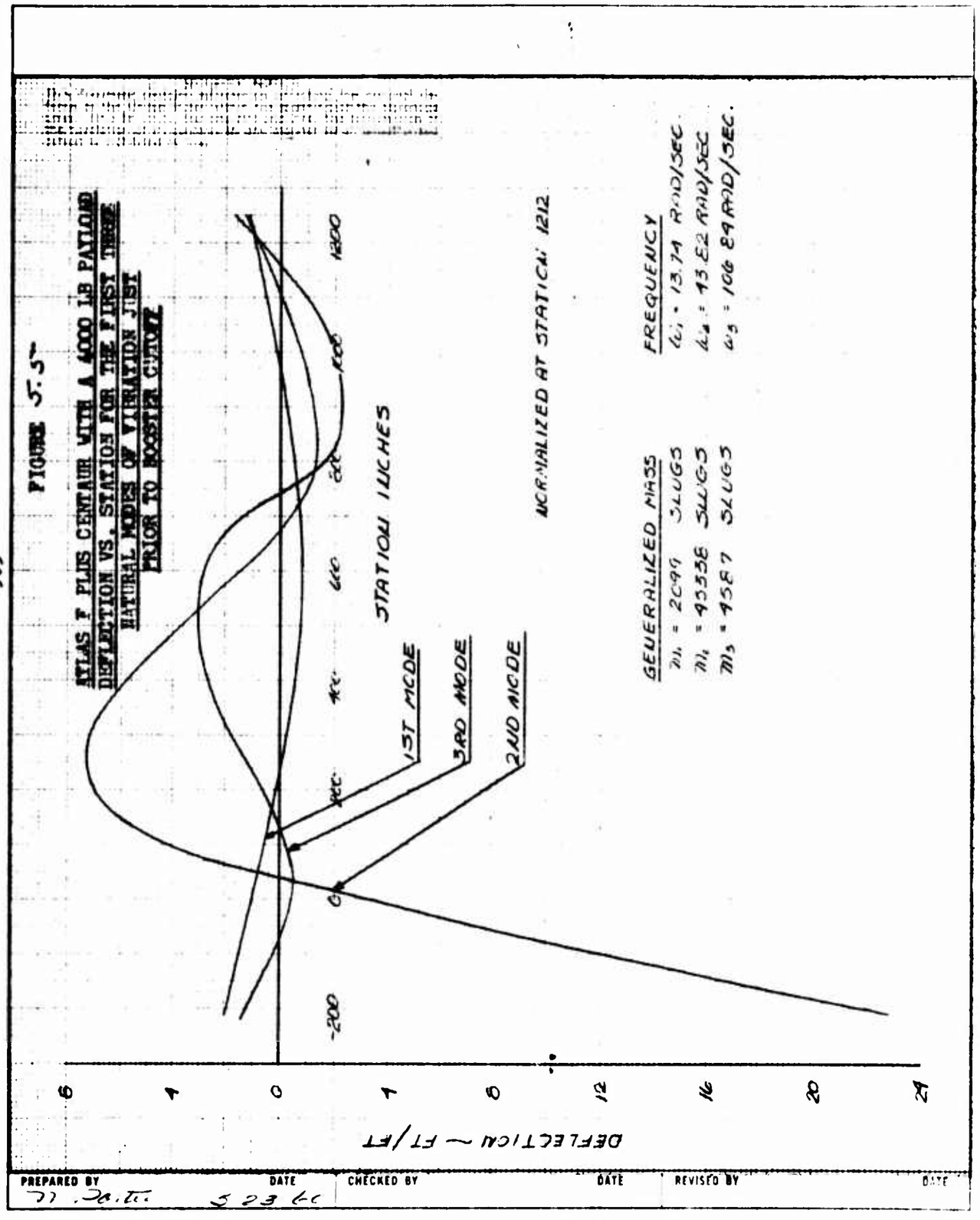

PREPARED BY	DATE	CHECKED BY	DATE	REVISED BY	DATE
[illegible]	5 23 60				

FORM NO. A1107-1

5.6

FIGURE 5.6

ATLAS F PLUS CENTAUR WITH A 17000 LB PAYLOAD
DEFLECTION VS. STATION FOR THE FIRST THREE
NATURAL MODES OF VIBRATION AT LAUNCH

GENERALIZED MASS	FREQUENCY
m_1 = 1967 SLUGS	ω_1 = 7.39 RAD/SEC
m_2 = 5019 SLUGS	ω_2 = 17.87 RAD/SEC
m_3 = 6269 SLUGS	ω_3 = 32.95 RAD/SEC

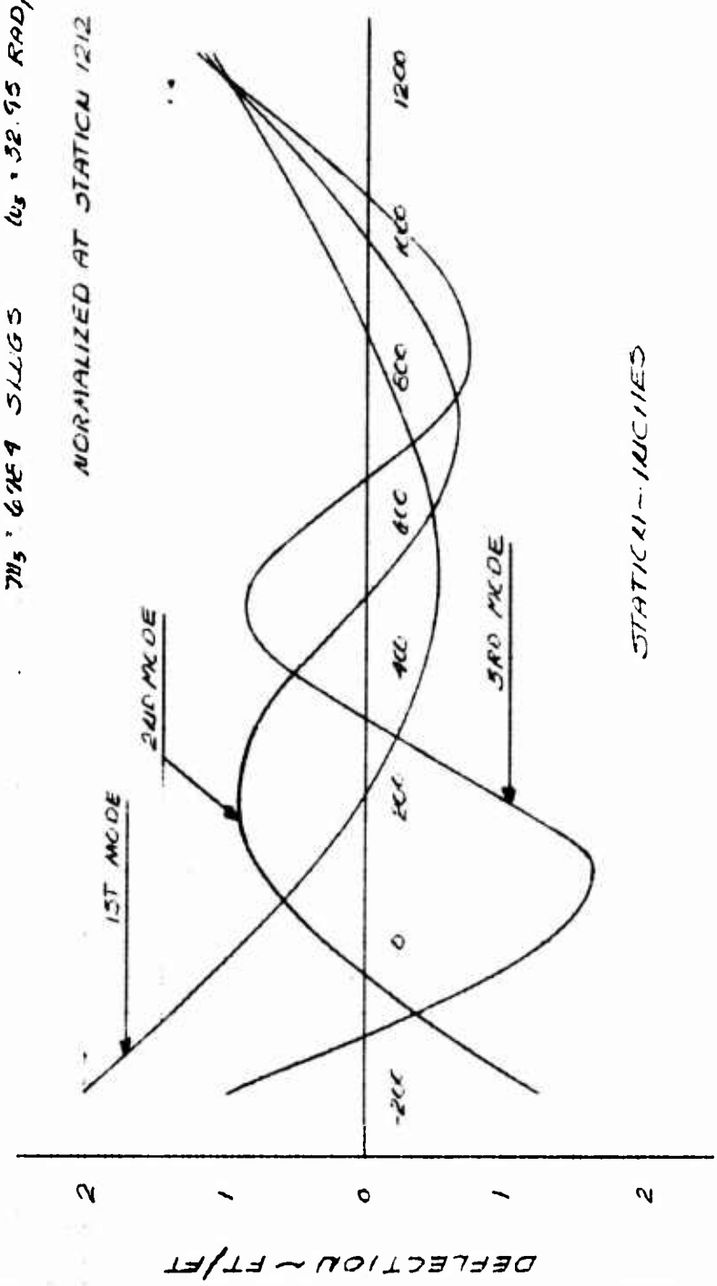

PREPARED BY	DATE	CHECKED BY	DATE	REVISED BY	DATE
M Pailet	5-23-60				

FORM NO. A1107-1

5.7

FIGURE 5.7

ATLAS F PLUS CENTAUR WITH A 17000 LB PAYLOAD
DEFLECTION VS. STATION FOR THE FIRST THREE
NATURAL MODES OF VIBRATION AT TIME OF MAX.
DYNAMIC PRESSURE

GENERALIZED MASS

$m_1 = 3936$ SLUGS

$m_2 = 10512$ SLUGS

$m_3 = 5659$ SLUGS

FREQUENCY

$\omega_1 = 7.86$ RAD/SEC.

$\omega_2 = 22.65$ RAD/SEC.

$\omega_3 = 39.05$ RAD/SEC.

NORMALIZED AT STATION 1212

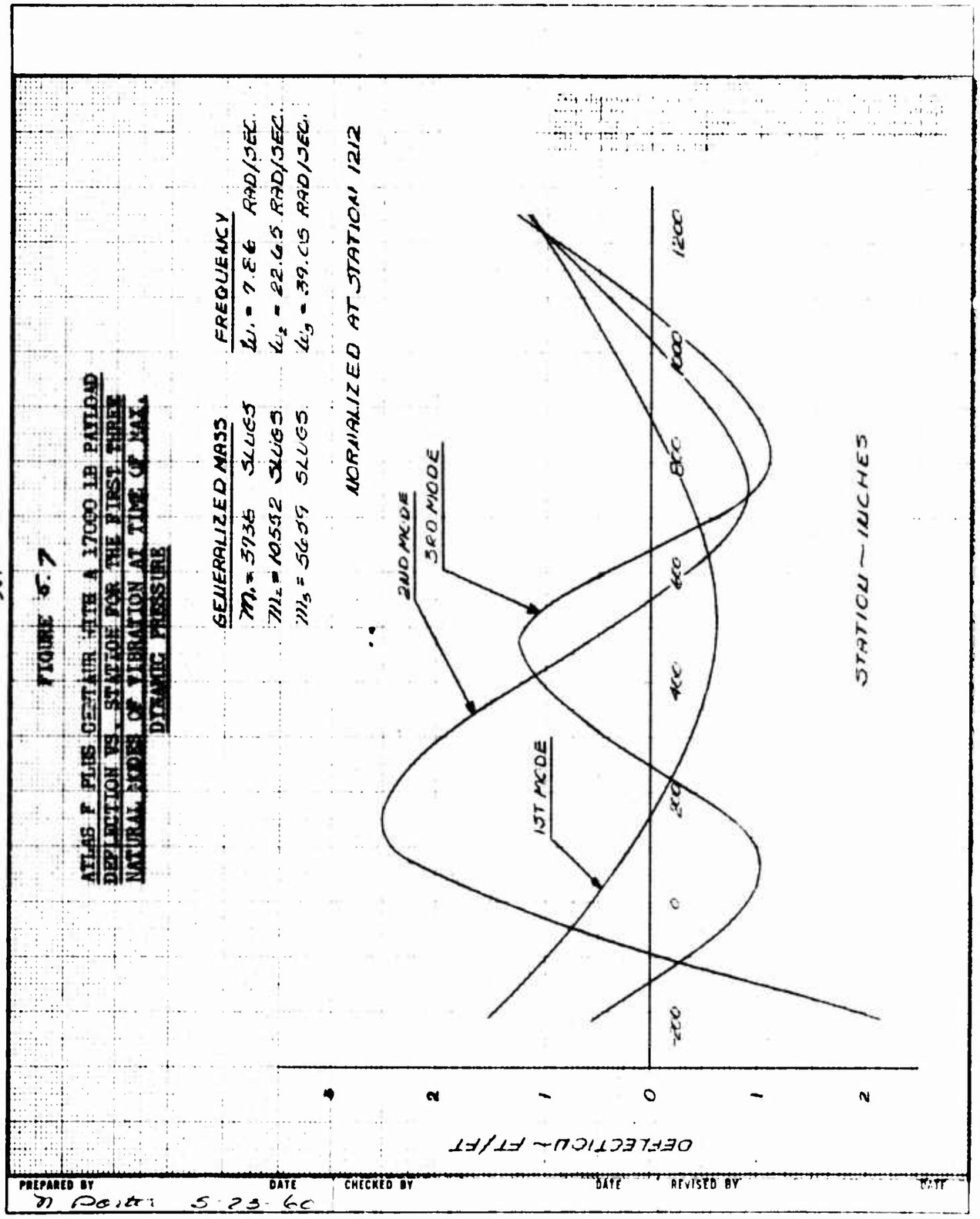

PREPARED BY M Poletti DATE 5-23-60 CHECKED BY DATE REVISED BY DATE

FORM NO. A1107-1

5.8

FIGURE 5.8

ATLAS F PLUS CENTAUR WITH A 17000 LB PAYLOAD
DEFLECTION VS. STATION FOR THE FIRST THREE
NATURAL MODES OF VIBRATION JUST PRIOR TO
BOOSTER CUTOFF

GENERALIZED MASS	FREQUENCY
m_1 = 2109 SLUGS	ω_1 = 16.75 RAD/SEC
m_2 = 6910 SLUGS	ω_2 = 23.95 RAD/SEC
m_3 = 9769 SLUGS	ω_3 = 165.95 RAD/SEC

NORMALIZED AT STATION 1212

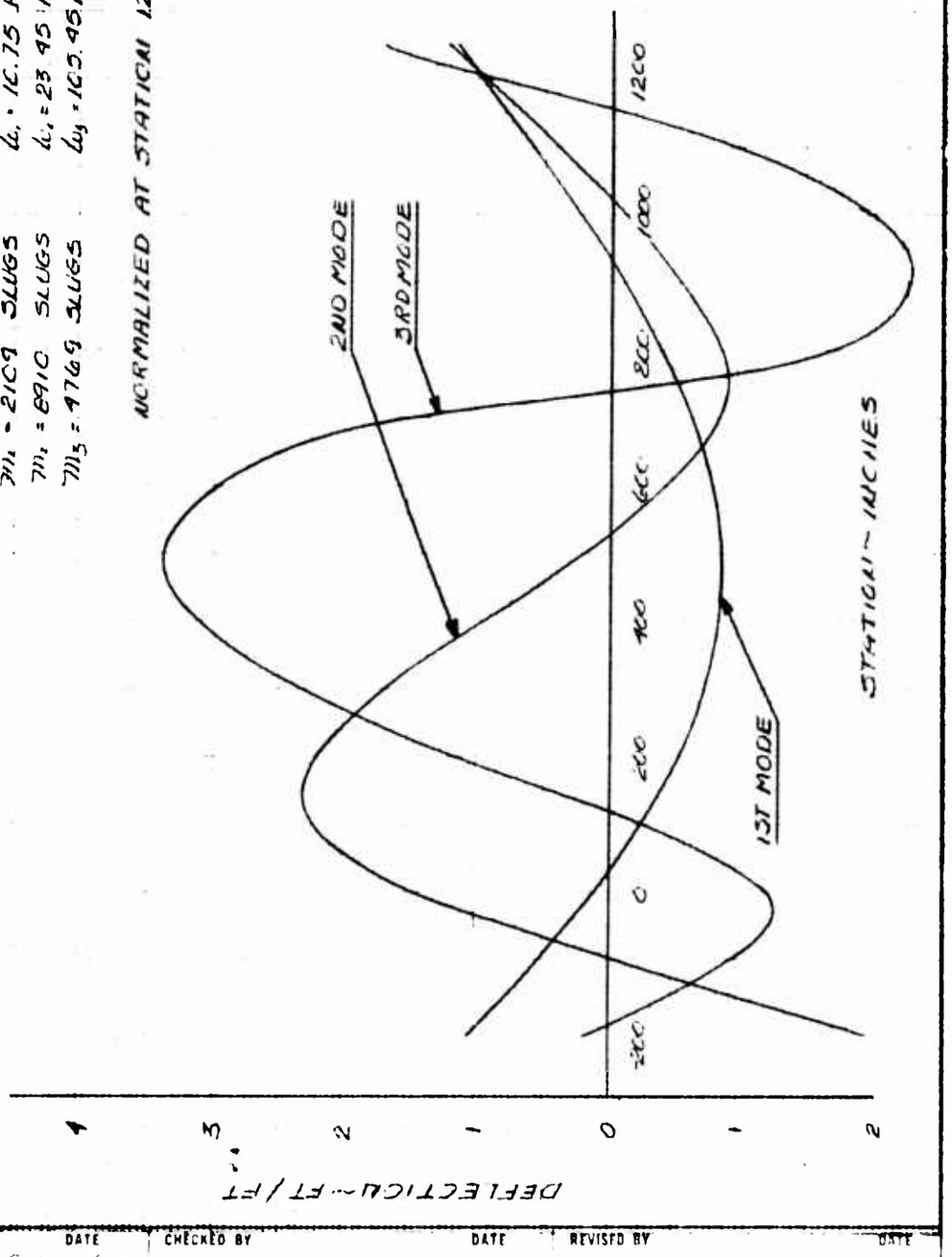

PREPARED BY [illegible] DATE Dec. 23 60 | CHECKED BY | DATE | REVISED BY | DATE

5.9

FIGURE 5.9

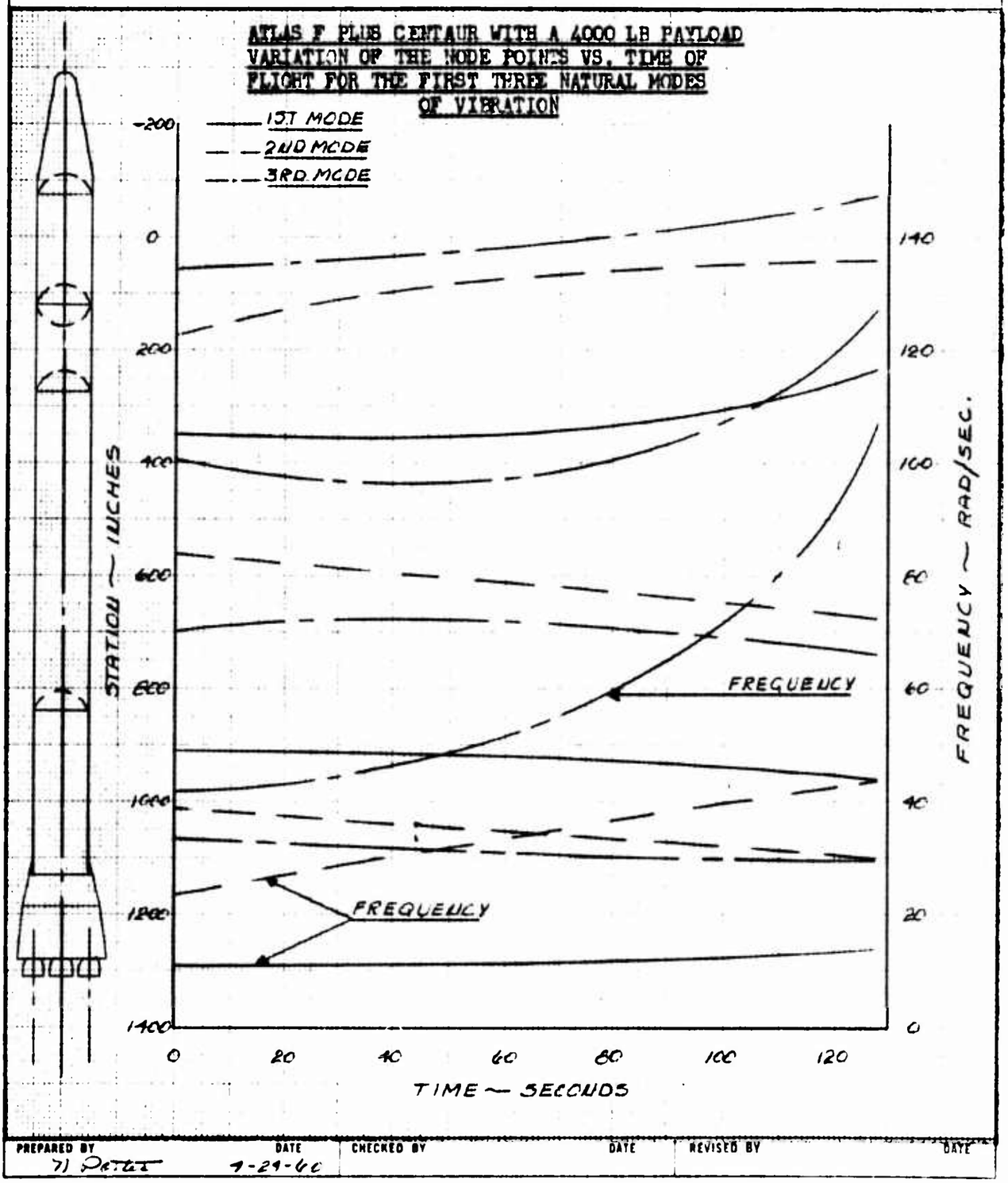

PREPARED BY	DATE	CHECKED BY	DATE	REVISED BY	DATE
TJ Pettet	9-29-60				

FORM NO. A1107-1

FIGURE 5.2.2

ATLAS F PLUS CENTAUR WITH A 17000 LB PAYLOAD
VARIATION OF THE MODE POINTS VS. TIME OF
FLIGHT FOR THE FIRST THREE NATURAL MODES
OF VIBRATION

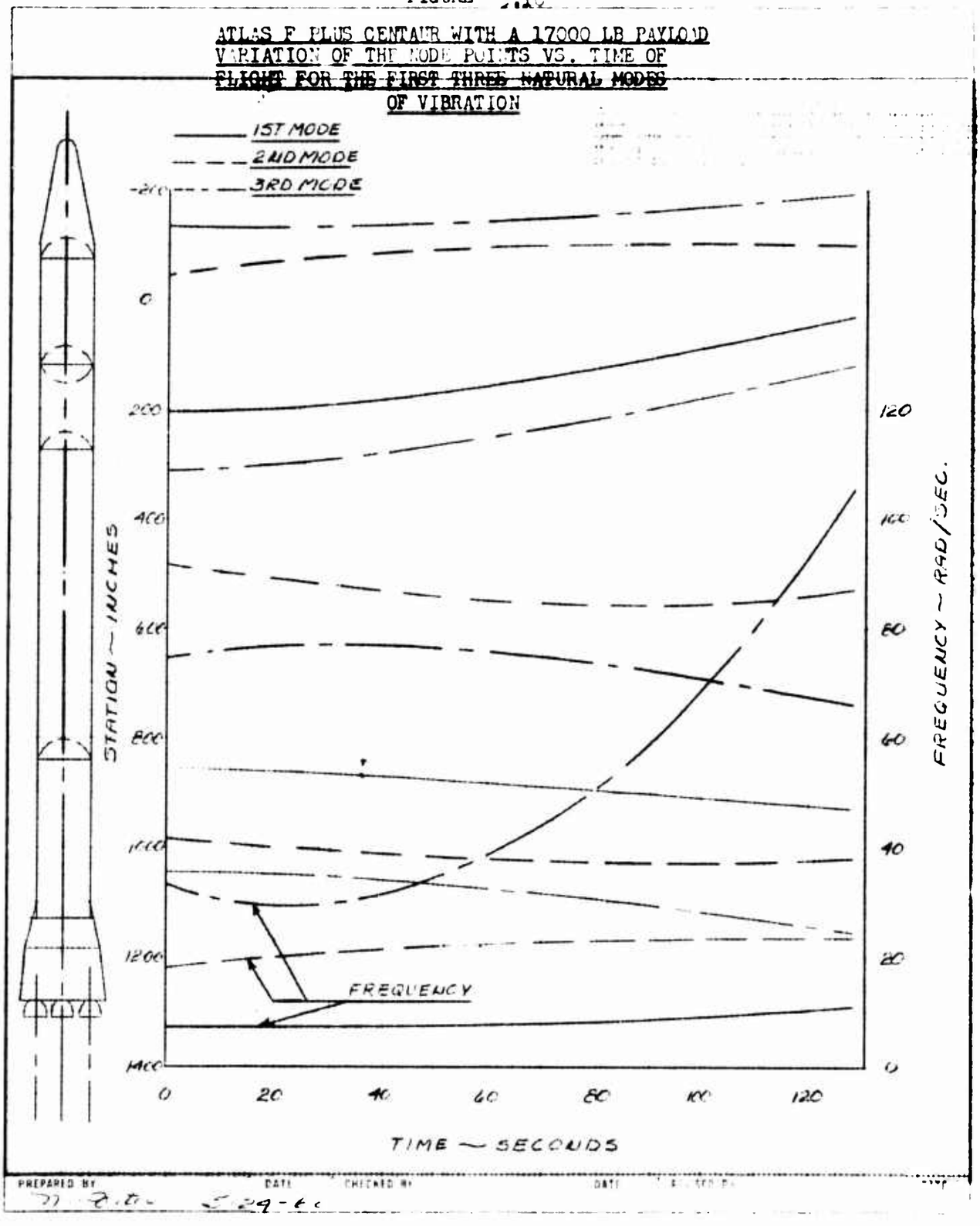

PREPARED BY DATE CHECKED BY DATE

FORM NO A1107-1

FIGURE 5.11

ATLAS F SERIES MISSILE VARIATION OF THE NODE POINTS VS. TIME OF FLIGHT FOR THE FIRST THREE NATURAL MODES OF VIBRATION

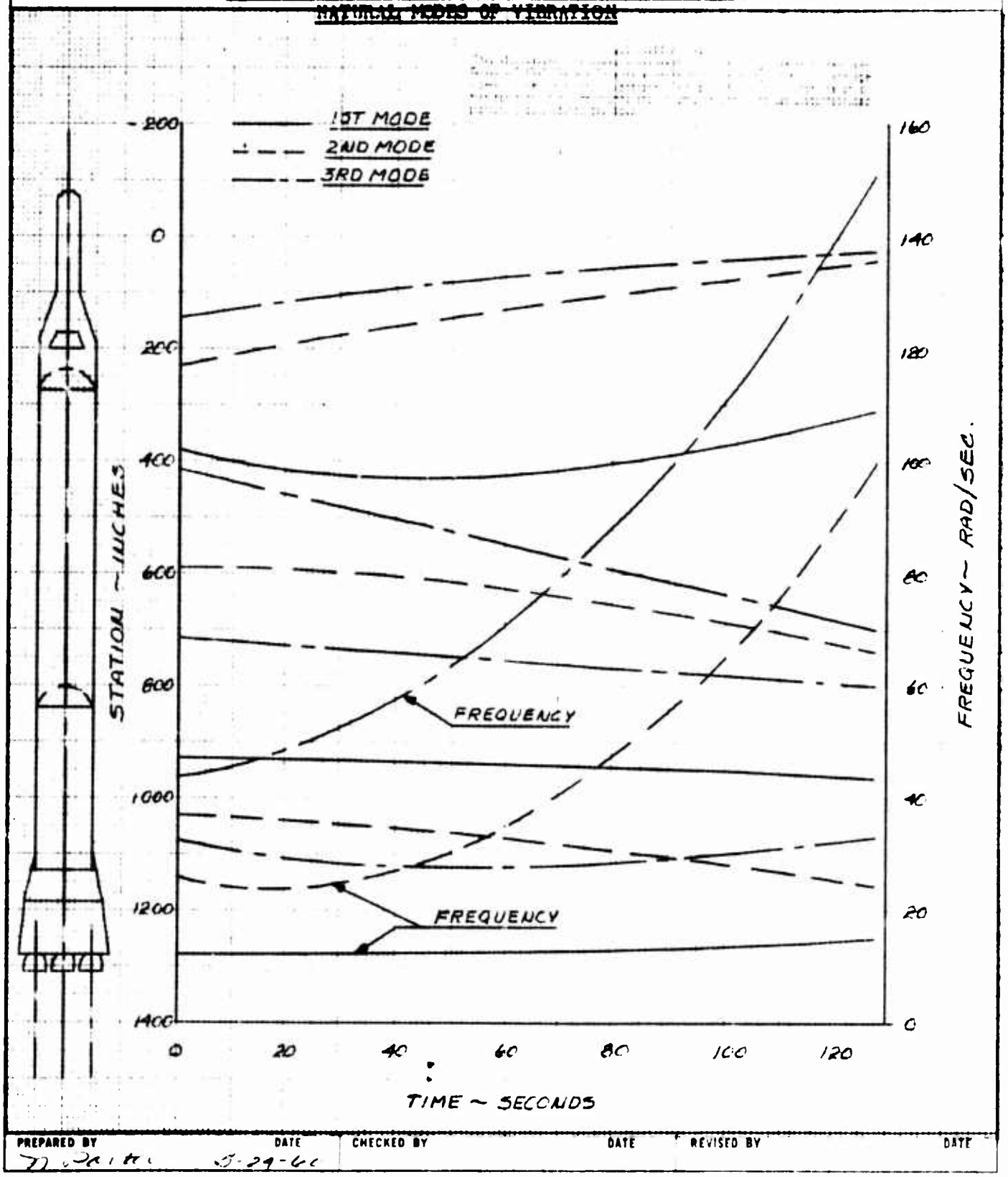

PREPARED BY	DATE	CHECKED BY	DATE	REVISED BY	DATE
D. Zahn	5-29-60				

FORM NO. A1107-1

control by rate and position gyro and pre-programmed flight path).

2. Lateral flight loads imposed by augmenting the configuration above with angle of attack or accelerometer feedback within the control loop.

The main purpose of the dual approach was, one, to determine if an augmented control system could sufficiently reduce the lateral flight loads on this vehicle so that an unmodified Atlas F ICBM structure could be directly utilized as a booster for this program, and two, the effect a comparison of the weight savings that are realized by an autmented system over a standard ICBM type control system.

To determine the lateral loads imposed on the vehicle during critical times of flight the following analyses were performed:

a) From optimized performance trajectories for both the 4000 pound and 17000 pound payload configurations the time of maximum dynamic pressure and its value were determined.

b) The vehicle was examined as a rigid body and the bending moment distribution for a unit angle of attack at this dynamic pressure was derived.

c) The total angle of attack that would be imposed on this vehicle when subjected to:

1. Operational winds - 1% risk wind profile and a normally applied 60 fps, (1-cos) type, gust (Fig.5.12 and 5.13).
2. 3 sigma AMR winds (Fig 5.12 and 5.13) and pre-programmed flight path so that the vehicle flies a zero angle of attack mean winter wind trajectory.
3. Same as (2) except using 2 sigma AMR winds (Fig 5.12 and 5.13).

The control system utilized in these studies was of the standard rate and position gyro type.

d) The angles of attack that would be imposed for the conditions listed in (c) augmenting the control system with an angle of attack or accelerometer feedback loop.

e) The following parameters were used in determining the maximum lateral loads along the length of the vehicle

Dyn. Pres.	Mach. No.	Velocity
750 psf	1.7	1300 fps

5.2.6 Standard Control System

Utilizing a standard rate and position gyro type control system the following criteria for angles of attack and engine control deflections imposed on both the 400 pound and 17000 pound payload versions were derived:

FIGURE 5.12 WIND PROFILES FOR VARIOUS PROBABILITIES OF OCCURENCE, INCLUDING OPERATIONAL CONDITIONS

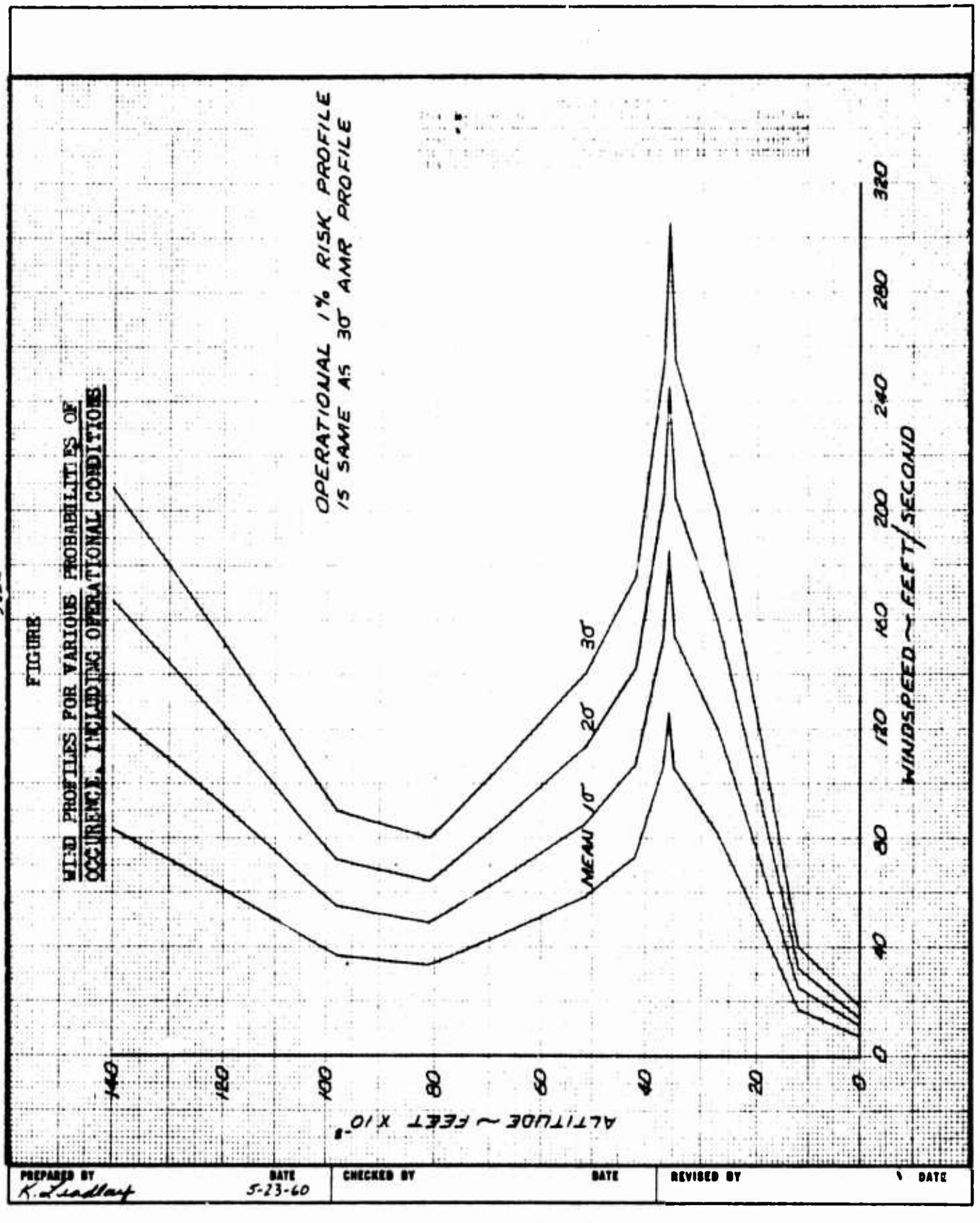

PREPARED BY	DATE	CHECKED BY	DATE	REVISED BY	DATE
K. Ludlam	5-23-60				

FIGURE 5.13

VARIATION OF GUST PROBABILITIES FOR AMP FOR VARIOUS PROBABILITIES OF OCCURRENCE AND FOR THE OPERATIONAL COURSE

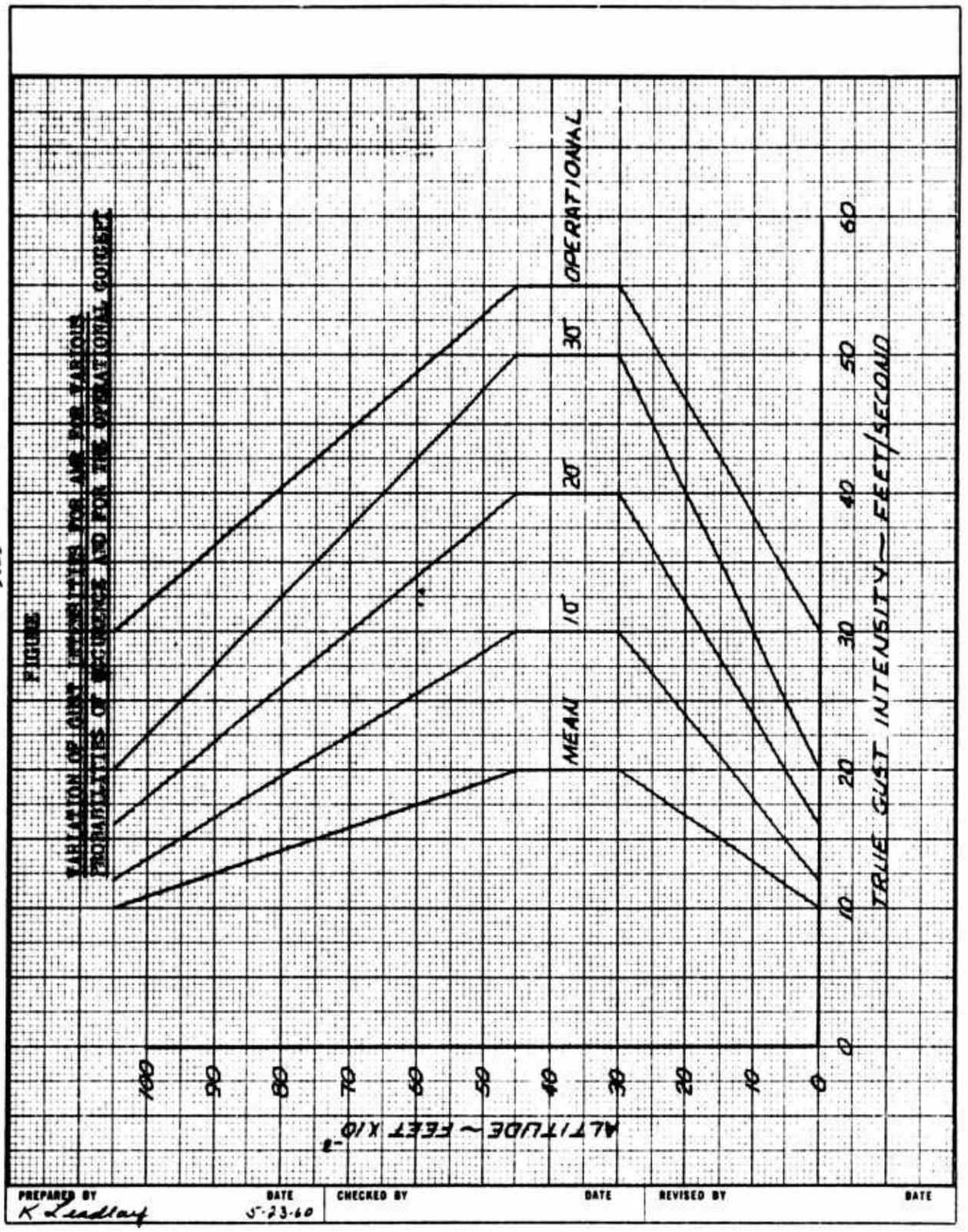

PREPARED BY	DATE	CHECKED BY	DATE	REVISED BY	DATE
K Leadley	5-23-60				

Wind Conditions	Payload	Angle of Attack		Required Eng. Deflection
		Steady State	Gust	
Operational	4000 lb.	4.5 deg.	2.64 deg.	4.08 deg.
	17000 lb.	4.5 deg.	2.64 deg.	3.55 deg.
3 sigma AMR	4000 lb.	3.3 deg.	2.2 deg.	3.16 deg.
	17000 lb.	3.3 deg.	2.2 deg.	2.75 deg.
2 sigma AMR	4000 lb.	2.2 deg.	1.76 deg.	2.0 deg.
	17000 lb.	2.2 deg.	1.76 deg.	2.0 deg.

The required engine deflections listed above do not include requirements for such static unbalances as thrust misalignment, geometrical alignment errors, c. g. offsets, etc. An additional allowance of approximately .75 degrees should be made for this purpose. The bending moment distribution is shown in Figures 5-14 through 5-19 for the various conditions. As can be seen by examination of these curves only the 2 sigma AMR wind conditions produce bending moments below the allowable bending moments on the unmodified Atlas F tank, For other wind conditions the Atlas F LO_2 tank would need increased pressure to accept these loads. Also for the 4000 pound payload version winds above 2 sigma AMR strength would require larger engine control deflections than are now presently available.

FIGURE 5.14

ATLAS F PLUS CENTAUR WITH A 4000 LB PAYLOAD
BENDING MOMENT VS. STATION AT TIME OF MAX $q\alpha$ #1

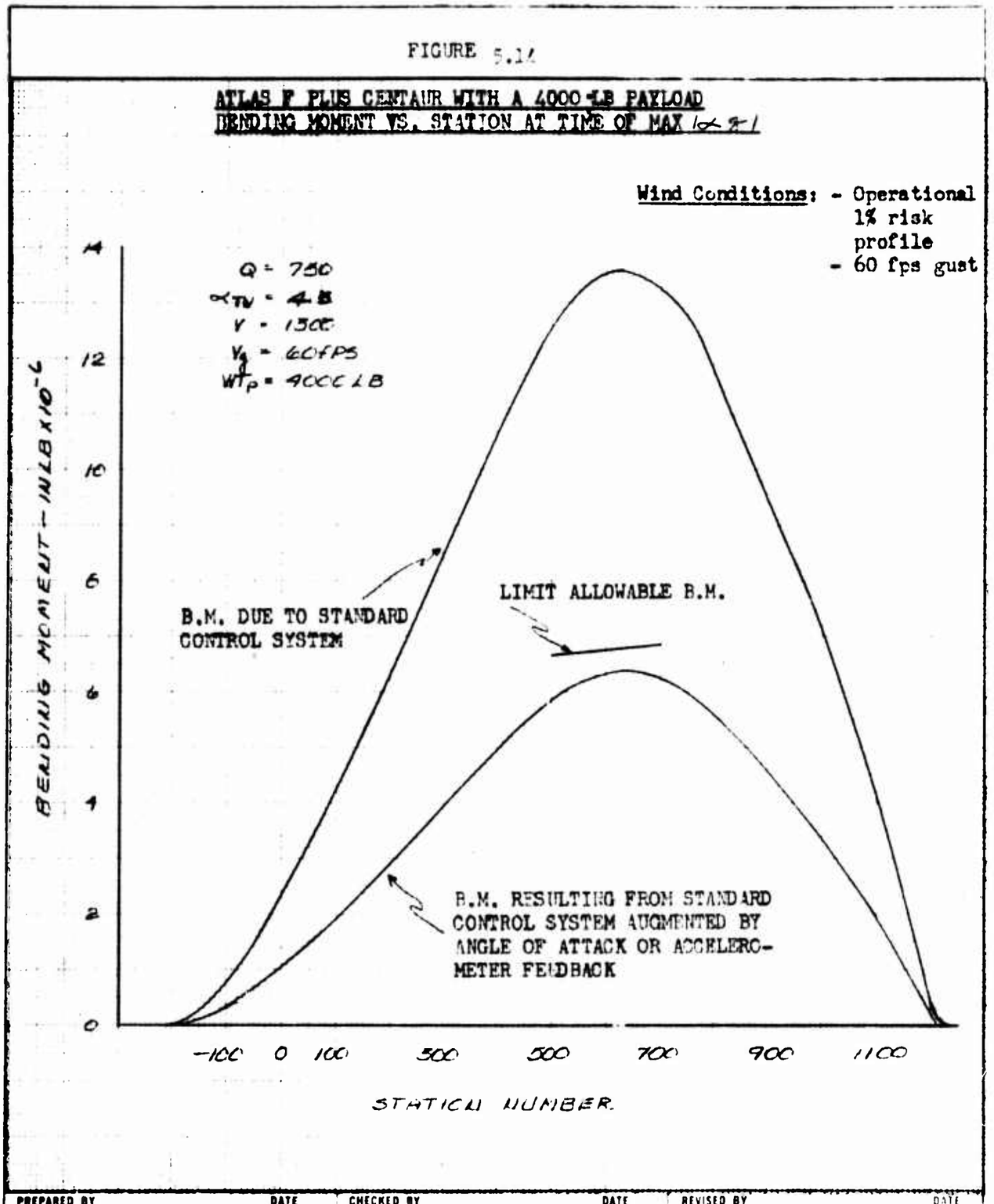

PREPARED BY	DATE	CHECKED BY	DATE	REVISED BY	DATE
N. Patel					

FIGURE 5.15

ATLAS F PLUS CENTAUR WITH A 4000 LB PAYLOAD
BENDING MOMENT VS. STATION AT TIME OF MAX (αq)

Wind Conditions: - 3 sigma
AMR profile
- 50 fps gust

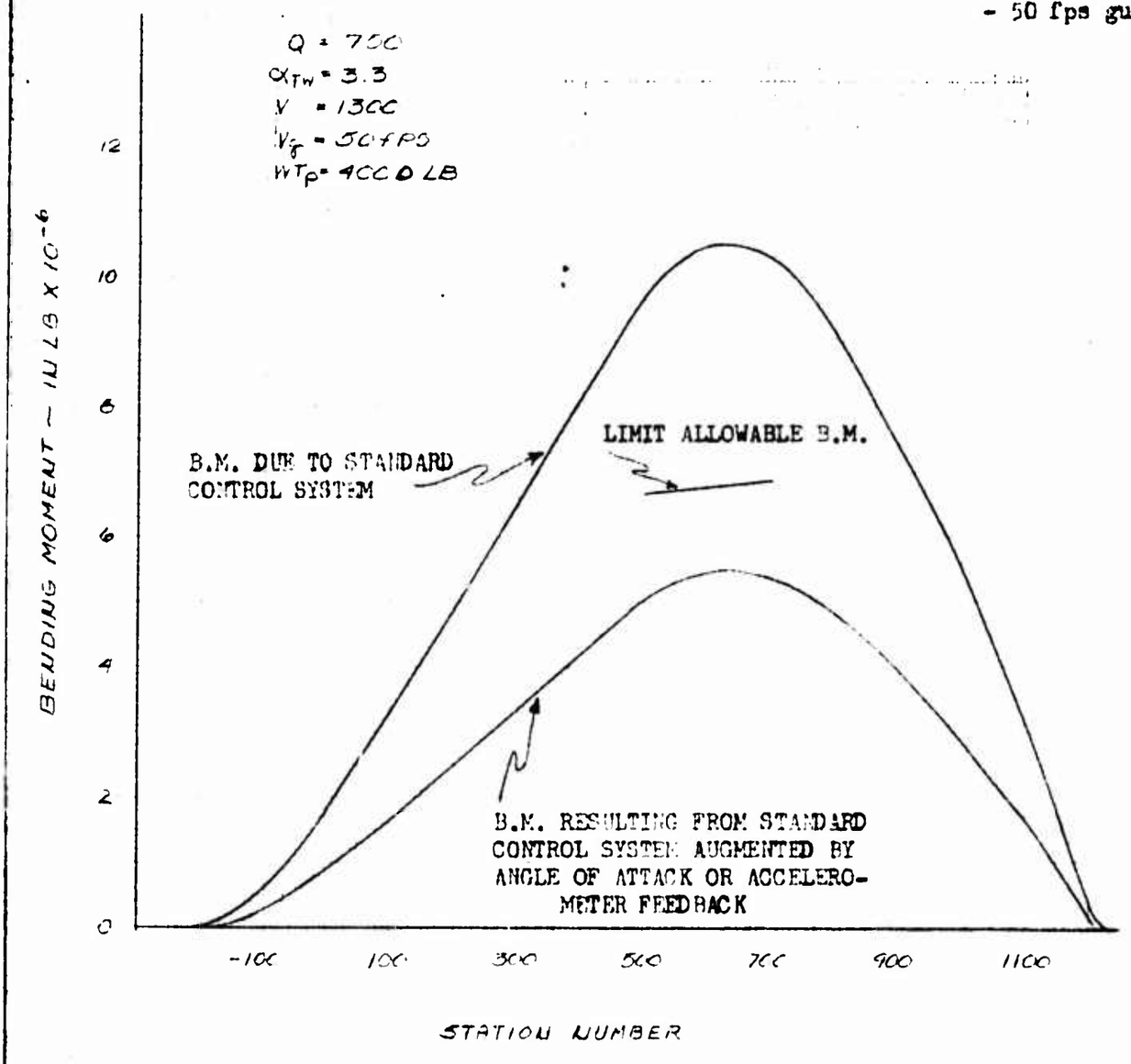

PREPARED BY	DATE	CHECKED BY	DATE	REVISED BY	DATE

FORM NO. A1107-1

FIGURE 5.1

ATLAS F PLUS CENTAUR WITH A 4000 LB PAYLOAD
BENDING MOMENT VS. STATION AT TIME OF MAX (αq)

Wind Conditions: - 2 sigma ATR profile
- 40 fps gust

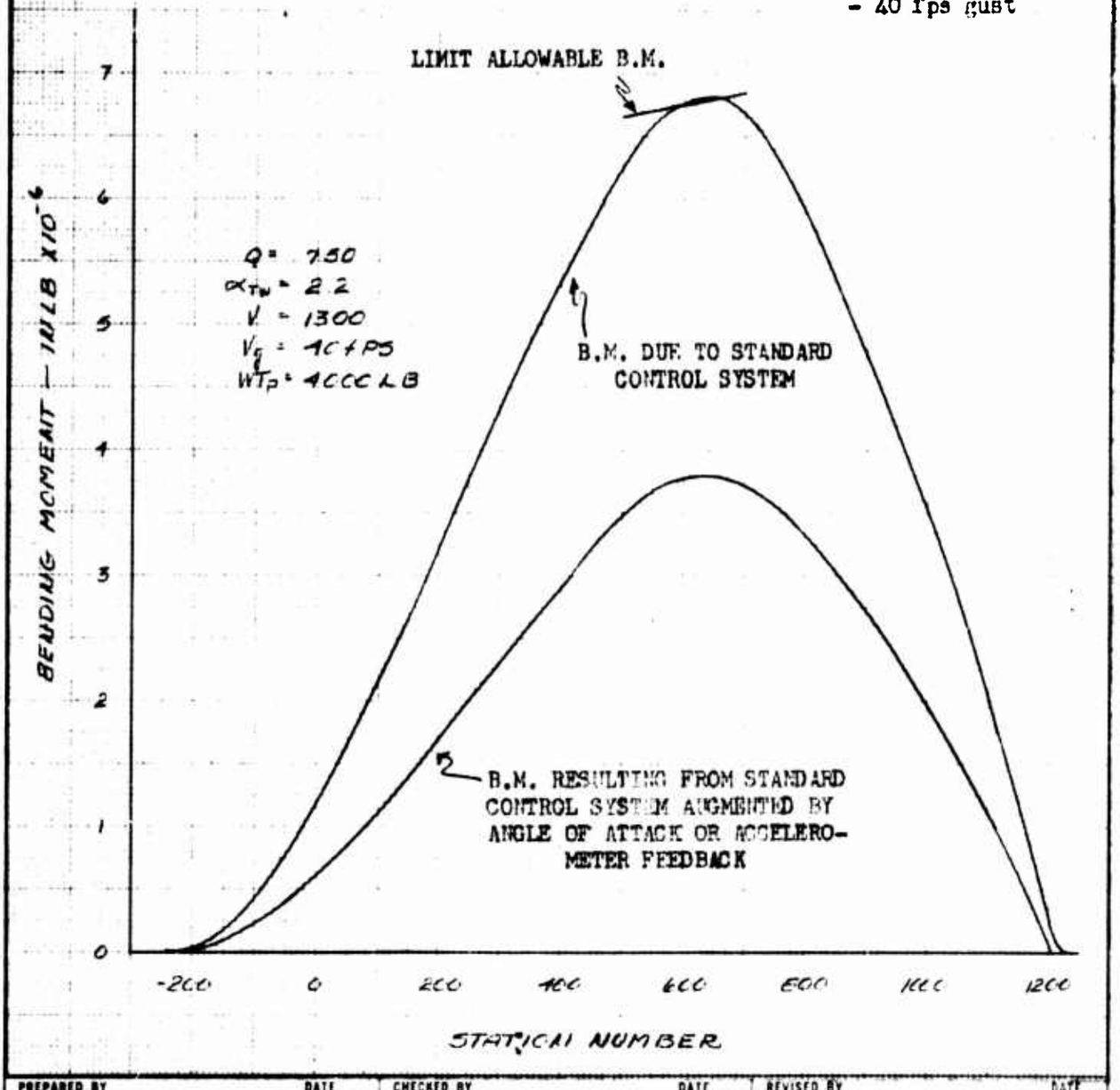

PREPARED BY	DATE	CHECKED BY	DATE	REVISED BY	DATE
J. Dr. DC					

FIGURE 5.17

ATLAS F PLUS CENTAUR WITH A 17000 LB PAYLOAD
BENDING MOMENT VS. STATION AT TIME OF MAX $1\alpha \bar{q}$

Wind Conditions: - Operational 1% risk profile
- 60 fps gust

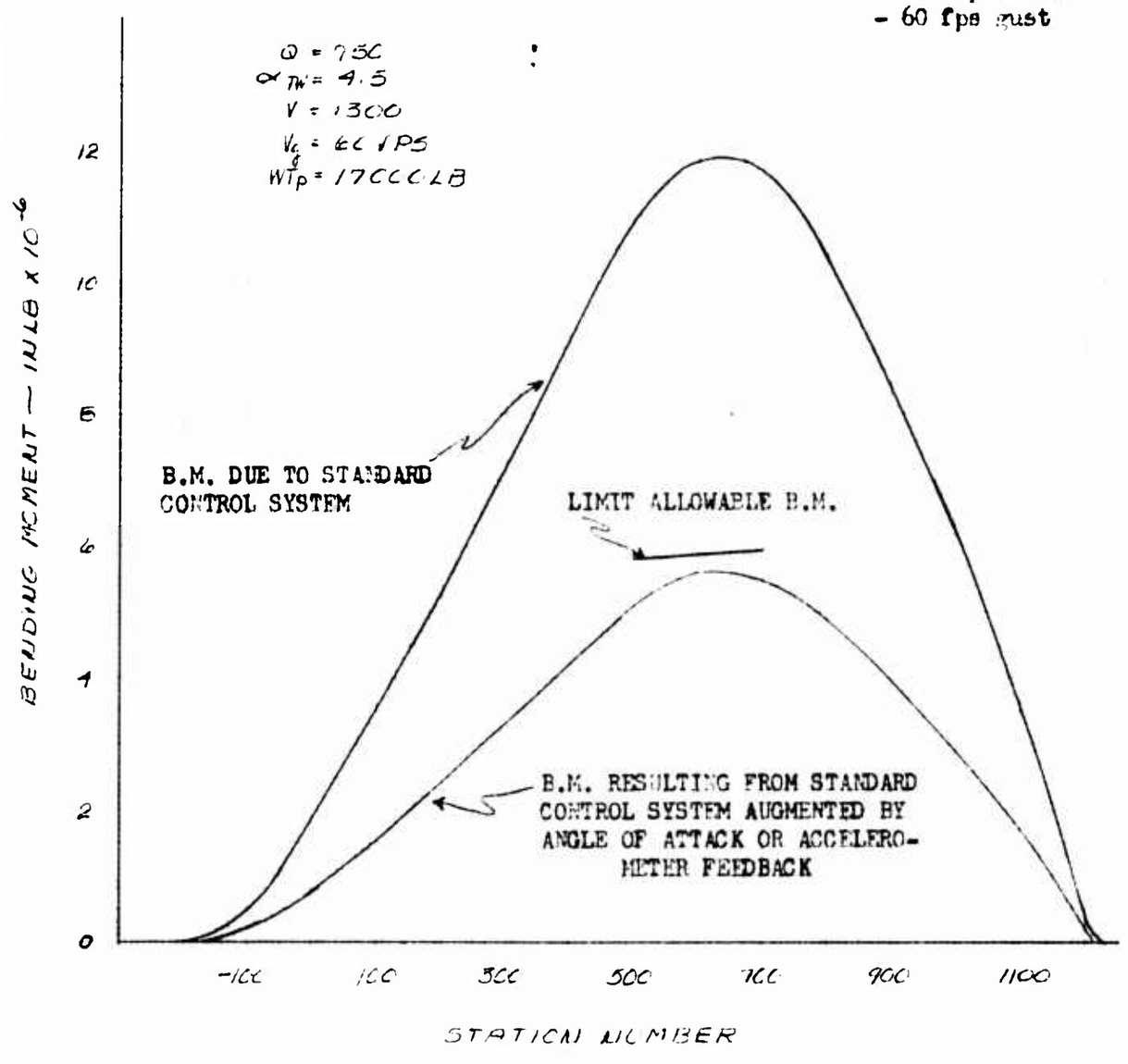

PREPARED BY DATE CHECKED BY DATE REVISED BY DATE

FORM NO. A1107-1

FIGURE 5.10

ATLAS F PLUS CENTAUR WITH A 17000 LB PAYLOAD
BENDING MOMENT VS. STATION AT TIME OF MAX (αq)

Wind Conditions: - 3 sigma AMR profile
- 50 fps gust

$Q = 750$
$\alpha_{T_B} = 5.3$
$V = 1300$
$V_q = 50$ FPS
$WT_p = 17000$ LB

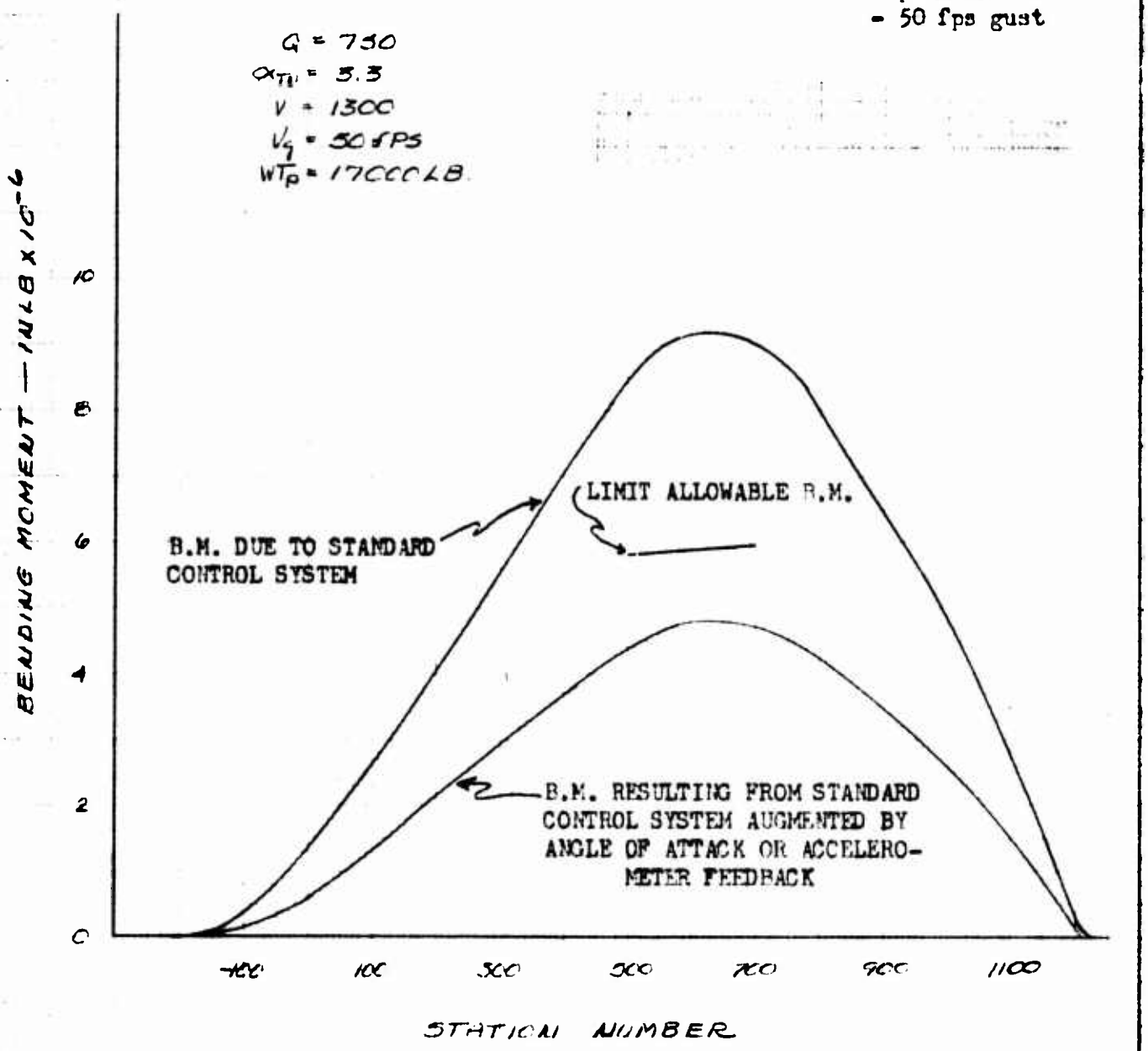

PREPARED BY	DATE	CHECKED BY	DATE	REVISED BY	DATE
[illegible]					

FORM NO. A1107-1

FIGURE 5.1-7

ATLAS F PLUS CENTAUR WITH A 17000 LB PAYLOAD
BENDING MOMENT VS. STATION AT TIME OF MAX $q\alpha$

Wind Conditions: - 2 sigma AMR profile
- 40 fps gust

$Q = 750$
$\alpha_{TW} = 2.2$
$V = 1300$
$V_{ij} = 40$ fps
$WT_p = 17000$ LB.

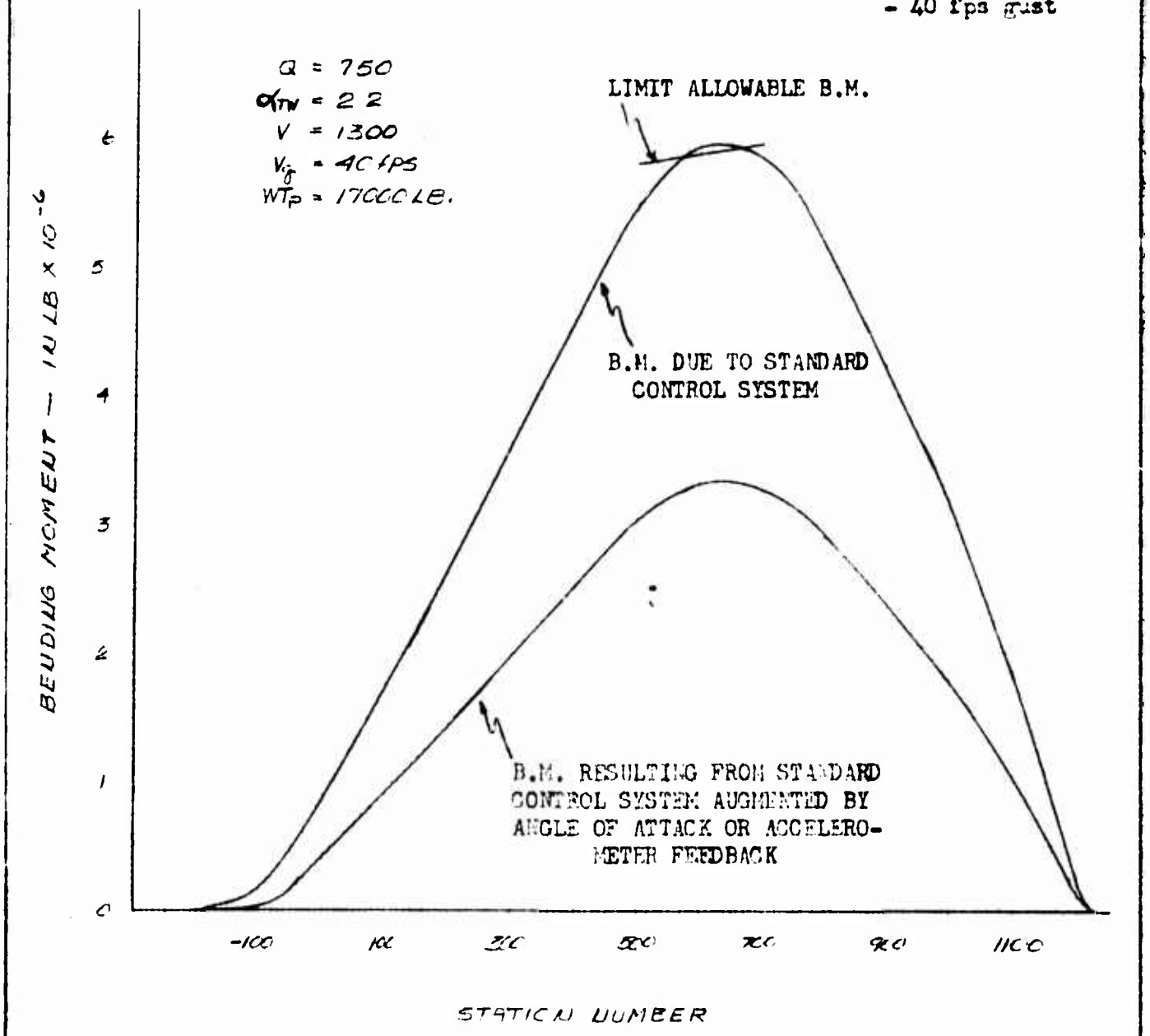

PREPARED BY [illegible] DATE CHECKED BY DATE REVISED BY DATE

FORM NO A1107-1

5.2.7 Standard Control System Augmented by Angle of Attack or Accelerometer Feedback

Utilizing the standard rate and position gyro control system augmented with an angle of attack or accelerometer feedback the following criteria for angle of attack and control engine deflections imposed on both the 4000 pound and 17,000 pound payload versions were derived:

Wind Condition	Payload	Angle of Attack		Required Eng. Deflection
		Steady State	Gust	
Operational	4000 lb.	.55 deg.	2.64 deg.	2.0 deg.
	17000 lb.	.55 deg.	2.64 deg.	1.75 deg.
3 sigma AMR	4000 lb.	.55 deg.	2.20 deg.	1.7 deg.
	17000 lb.	.55 deg.	2.20 deg.	1.5 deg.
2 sigma AMR	4000 lb.	.55 deg.	1.76 deg.	1.45 deg.
	17000 lb.	.55 deg.	1.76 deg.	1.25 deg.

The bending moment distribution is shown in Figures 5.14 through 5.19 for the various conditions.

The details of the actual control equations utilized for the angle of attack or accelerometer feedback loop can be found in the section on Dynamic Stability and Control. A resume of the features afforded in relieving the loading on the vehicle are:

1. Either syster will, in essence, tend to weather cock the vehicle into the prevailing wind thus reducing the imposed angle of attack.

2. Since either system has an integral term it was felt that not less than 1/2 degree angle of attack could be realized. Instrumentation accuracies over the desired dynamic pressure and Mach. No. regions was assumed to be .05 degrees.

3. Although alleviation of the gust angle of attack will certainly be realized with either system no account of such a reduction was accounted for in this study. This will tend to make the results conservative.

4. Augmentation of angle of attack or accelerometer control with other systems', such as the inertial guidance system, was not attempted in this study.

The results of this area of investigation has shown that the Atlas F missile as designed for an ICBM could be utilized as the booster for the Centaur + Payload combinations described without modification for lateral flight loads. Conservatism in the approach has been utilized in all these studies.

6.0 Stability and Control

6.1 Introduction

Stability and control studies of the Atlas F as a space booster were performed using an Atlas F plus Centaur configuration with various payloads. A primary area of investigation was the use of auxiliary feedback loops employing either angle of attack or acceleration feedback to reduce the steady-state angle of attack at maximum dynamic pressure and thus achieve a reduction in the lateral loads on the missile. Such a system is proposed and its feasibility is demonstrated. Additional studies were performed to determine the stability qualities of the vehicle when coupled with the lateral bending modes and sloshing propellants. Root loci are presented to show that no stability problems are encountered due to bending or sloshing.

The basic autopilot configuration proposed for the Atlas F - Space Booster is identical to the Atlas F except for consideration of an auxiliary feedback loop for load relief. The position reference was assumed to be a position gyro, located at the same position as the rate gyros on the missile (Station 975 - the same as on the F). Very likely the position reference, in practice, will be obtained from the guidance system. For analysis purposes, however, a position gyro was used since the guidance system is not specified in detail. This assumption has a negligible effect

upon the results. Figure 6.1 shows a block diagram of the basic autopilot configuration. Nomenclature and sign conventions used are shown in Figure 6.2

6.2 Auxiliary Feedback Loop for Load Reduction

In the section on dynamic loads, it was pointed out that an unmodified Atlas F tank is adequate for those structural requirements imposed by two sigma AMR wind conditions. To provide the capability of flying the Atlas F plus Centaur plus payload for operational wind criteria without resorting to higher Atlas LO_2 tank pressures and consequent increase in weight, the use of either angle of attack or acceleration feedback to reduce steady state angle of attack is proposed. These feedback loops are shown in the block diagram of Figure 6.1 by dotted lines.

As the vehicle rises through the atmosphere on its trajectory, it is subjected to varying wind velocities of the wind conditions that result in the vehicle acquiring an angle of attack. The variation of the wind conditions with altitude is referred to as a wind profile, Since the wind conditions vary slowly, the angle of attack resulting from the wind profile is called the steady state angle of attack (as opposed to the rapid variations in angle of attack arising from wind gusts). The primary purpose of the load alleviation devices is to reduce the steady angle of attack by turning the vehicle into the wind. Both types of auxiliary feedback

MISSILE AND CONTROL SYSTEM BLOCK DIAGRAMS
WITH AUXILIARY FEEDBACK LOOPS

FIGURE 6.1

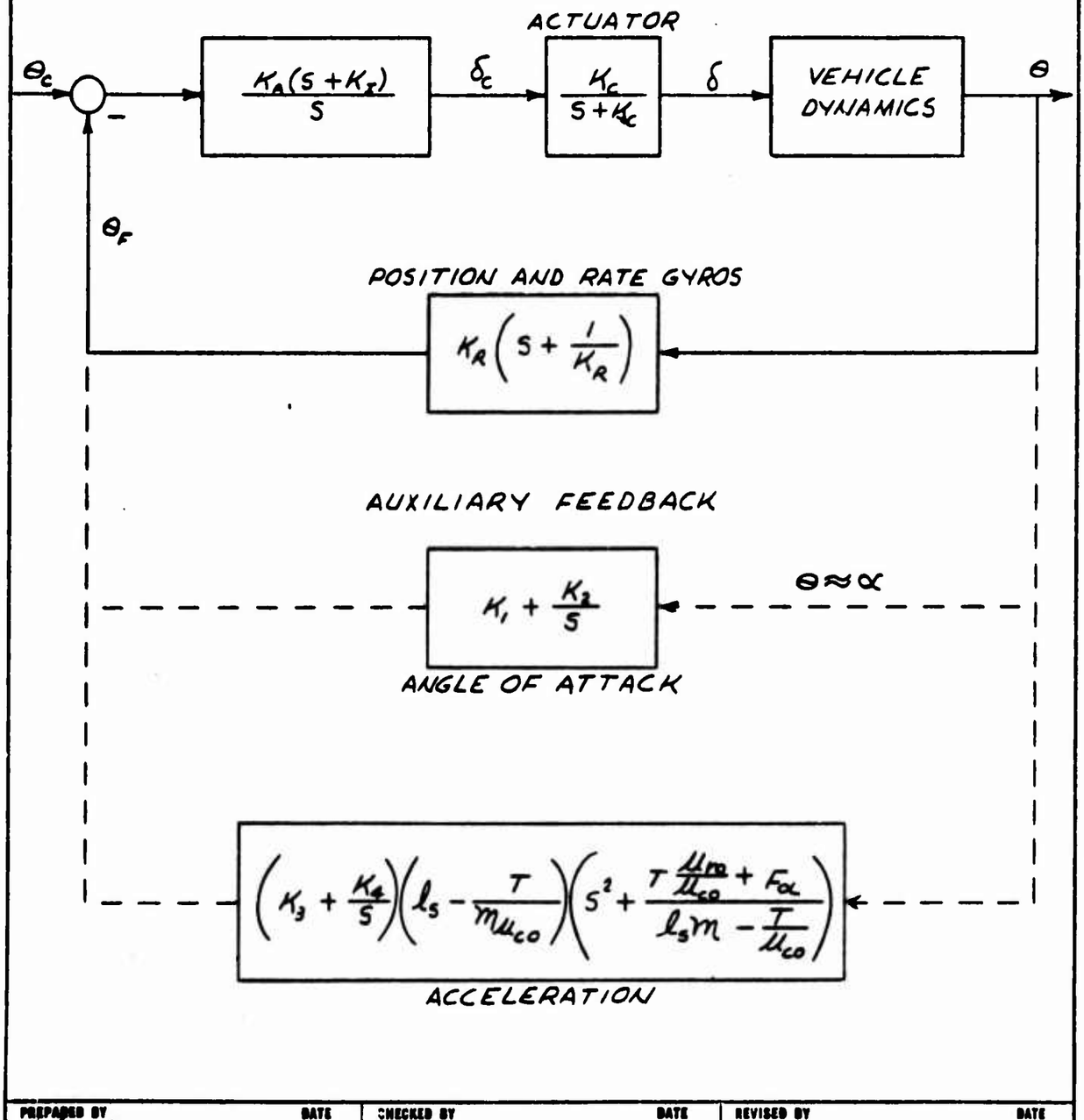

PREPARED BY	DATE	CHECKED BY	DATE	REVISED BY	DATE
K. Leadley	5-24-60				

FIGURE 6.2

NOMENCLATURE AND SIGN CONVENTIONS

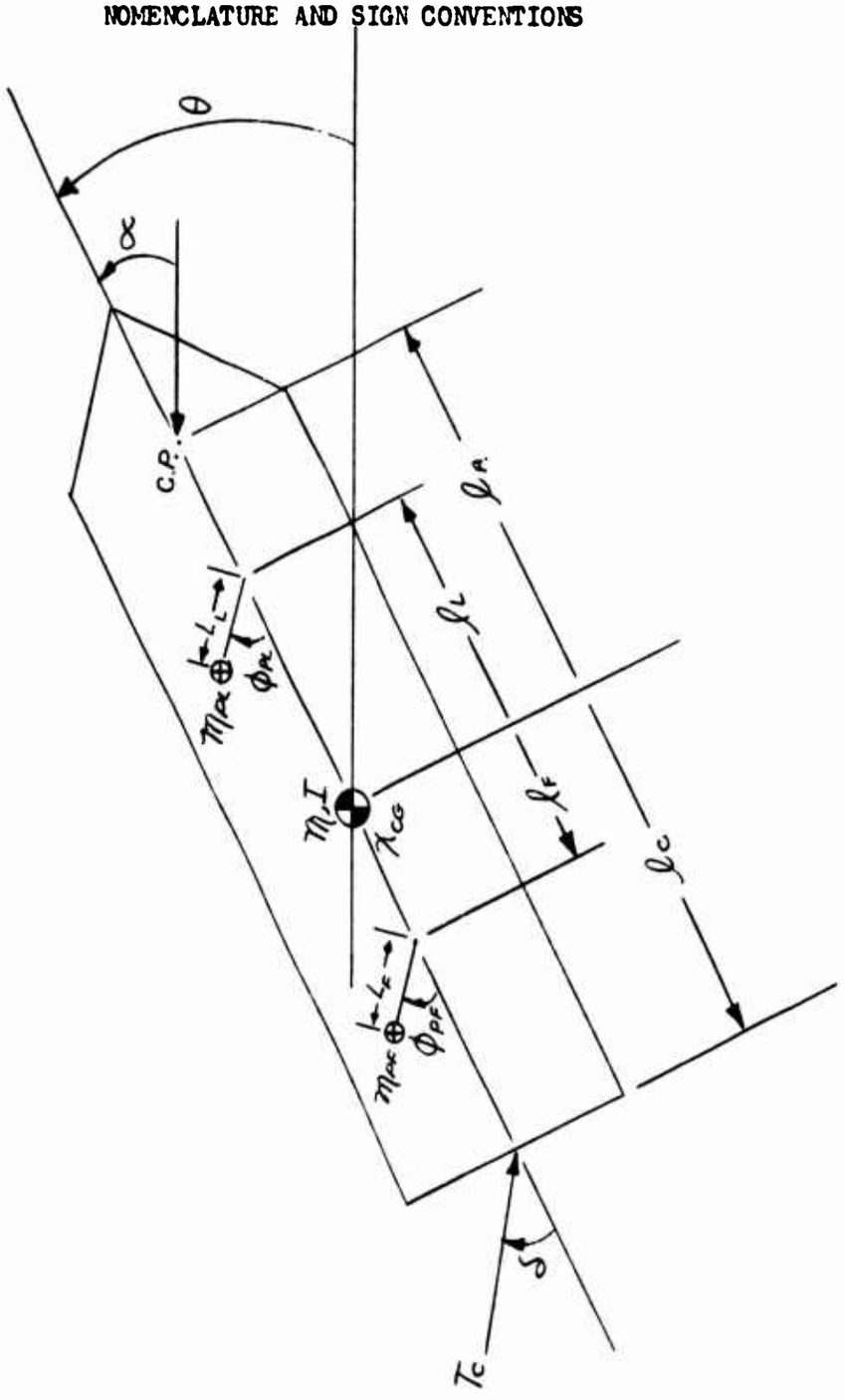

PREPARED BY	DATE	CHECKED BY	DATE	REVISED BY	DATE

have an integral term $\frac{K}{S}$ (see Figure 6.1) which causes the steady state angle of attack to approach zero. A constant gain term in the auxiliary feedback loop is also included to recover the deterioration in system stability caused by the integral term.

The auxiliary feedback loop is proposed to be activated at approximately forty-five seconds, which is 15 to 20 seconds before the vehicle reaches maximum dynamic pressure. Time varying analog simulations have shown that introducing the angle of attack or acceleration feedback at this time reduces the steady state angle of attack to 0.5 degrees at the time of maximum dynamic pressure. In addition, this auxiliary loop provides from 15 to 20 per cent reduction in the bending moment on the vehicle due to gusts. After passing through the region of high dynamic pressure the auxiliary loop should be deactivated to reduce lateral drift errors.

The root locus of the system including angle of attack feedback is shown in Figure 6.3 and demonstrates that the system is stable for practical values of gains. The root locus of the system including acceleration feedback is shown in Figure 6.4. All the roots are in the LHP and thus, the optimum gain for steady-state angle of attack reduction can be achieved.

Thus, both systems provide relief of loads due to angle of attack at maximum dynamic pressure. Selections of one system over the other depends primarily on practical consideration of ease of

FIGURE 6.3

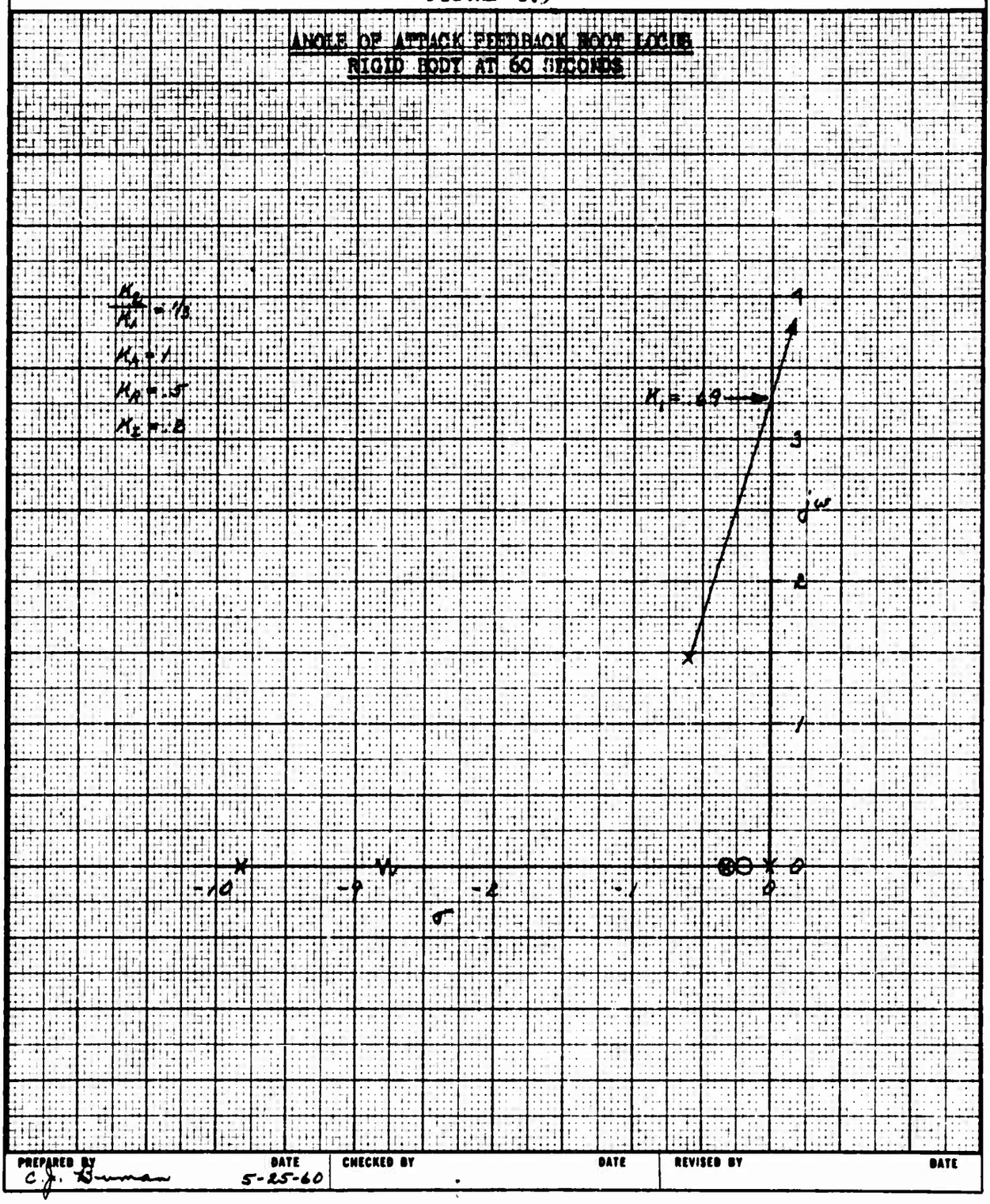

PREPARED BY C. J. Burman DATE 5-25-60 | CHECKED BY DATE | REVISED BY DATE

FIGURE 6.4

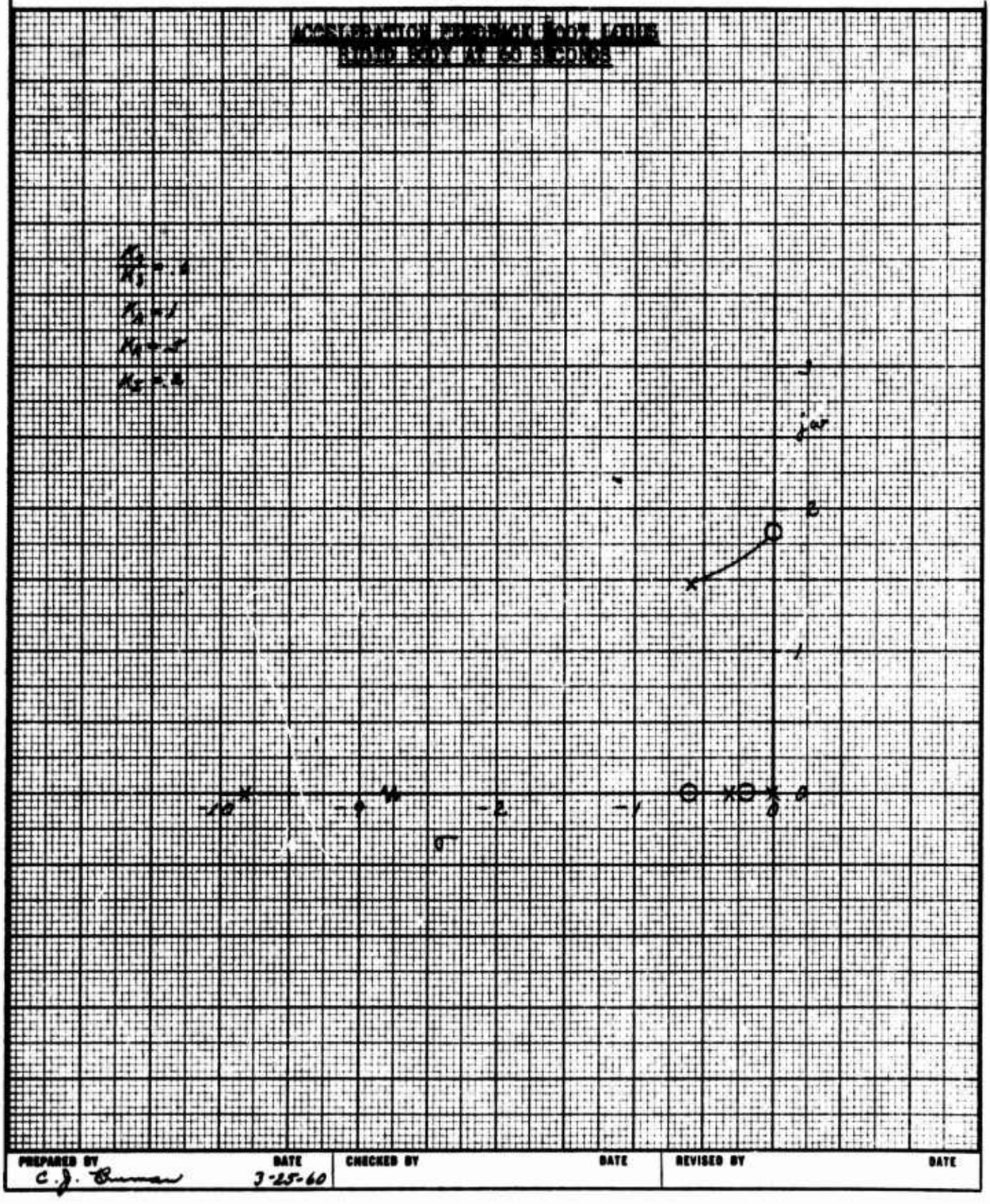

PREPARED BY	DATE	CHECKED BY	DATE	REVISED BY	DATE
C. J. Burman	3-25-60				

mechanizing each type and on the influence of each type on higher frequency modes. The accelerometer feedback, in particular, will require analysis to determine its effect on bending modes.

6.3 Elastic Coupling

Studies of the elastic coupling of the first three bending modes with the autopilot are based on the model shown in the block diagram of Figure 6.5 This model in turn is a simplification of the system equations developed in Reference A. This model does not include the effects of sloshing or aerodynamics. Coupling of the bending modes into the autopilot system is through the position and rate gyros.

6.4 Analysis Techniques

The results of this investigation are presented as root loci in Figures 6.6, 6.7 and 6.8 for the first, second, and third modes, respectively at three time instants of booster flight - launch, 60 second, and 128 seconds. The transfer function of the actuator used in this study is also shown in Figure 6.5. (A Bode plot of the actuator phase and amplitude characteristics is shown in Report AE 60-0355). The roots for these loci were obtained by means of a digital solution of the system equations represented in Figure 6.5. While this method provides a quick method of acquiring stability data, little insight into the problem of what affects stability is obtained from these data alone. A more

CONVAIR ASTRONAUTICS

FIGURE

MISSILE AND CONTROL SYSTEM WI

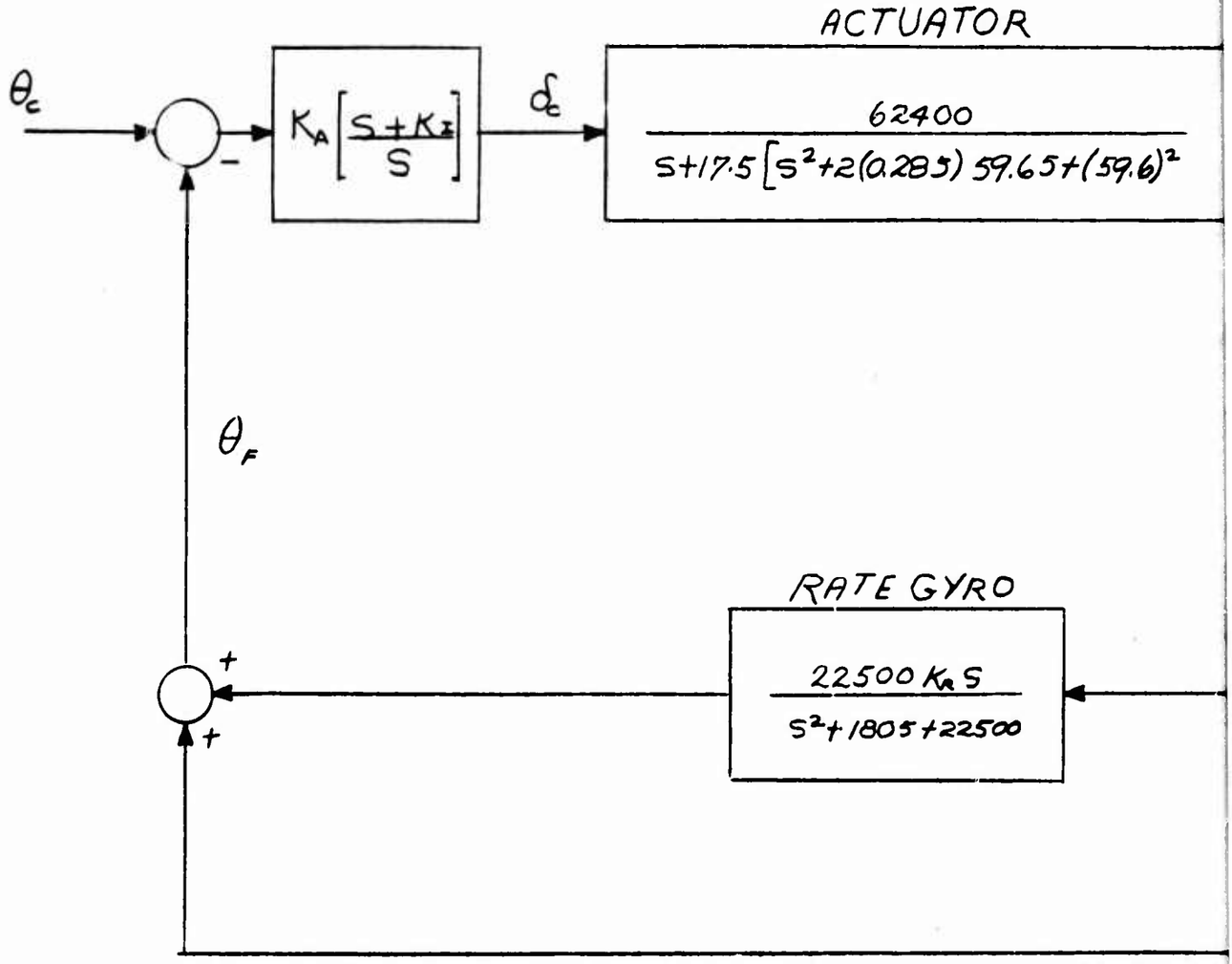

$m_{(i)}$ generalized mass of the i^{th} mode slugs
$\omega_{(i)}$ modal frequency of the i^{th} mode
$\phi_x^{(i)}$ slope of the i^{th} mode at sta x
$\ell_R m_R \sum \ell_R m_R$ of the gimbaled engines
$I_R \sum I_R$ of the gimbaled engines

A

FORM NO. A706-4

FIGURE 6.5
SYSTEM WITH ELASTIC COUPLING

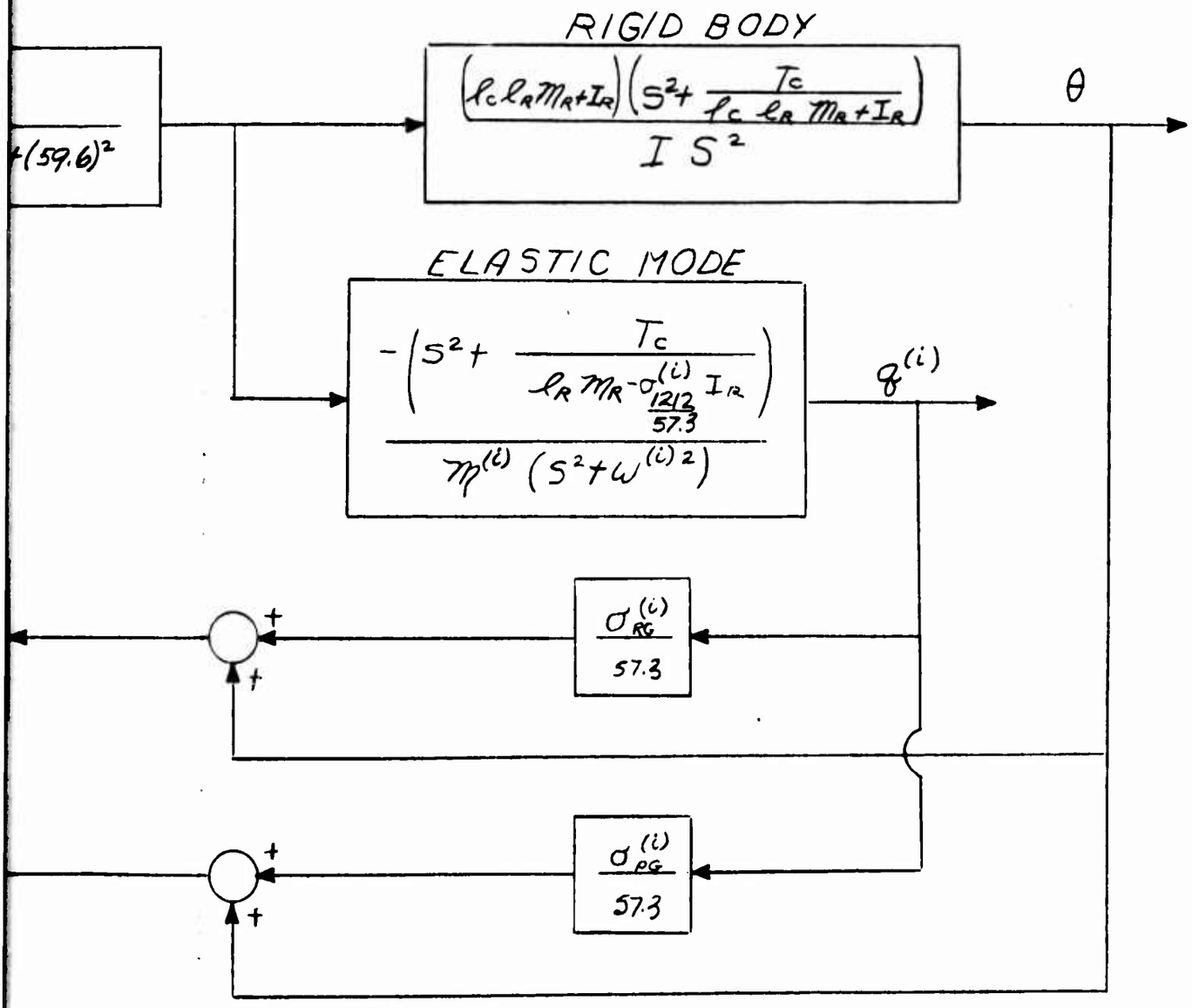

	PREPARED BY	DATE	CHECKED BY	DATE	REVISED BY	DATE

FIGURE 6.6

1ST MODE ROOT LOCI

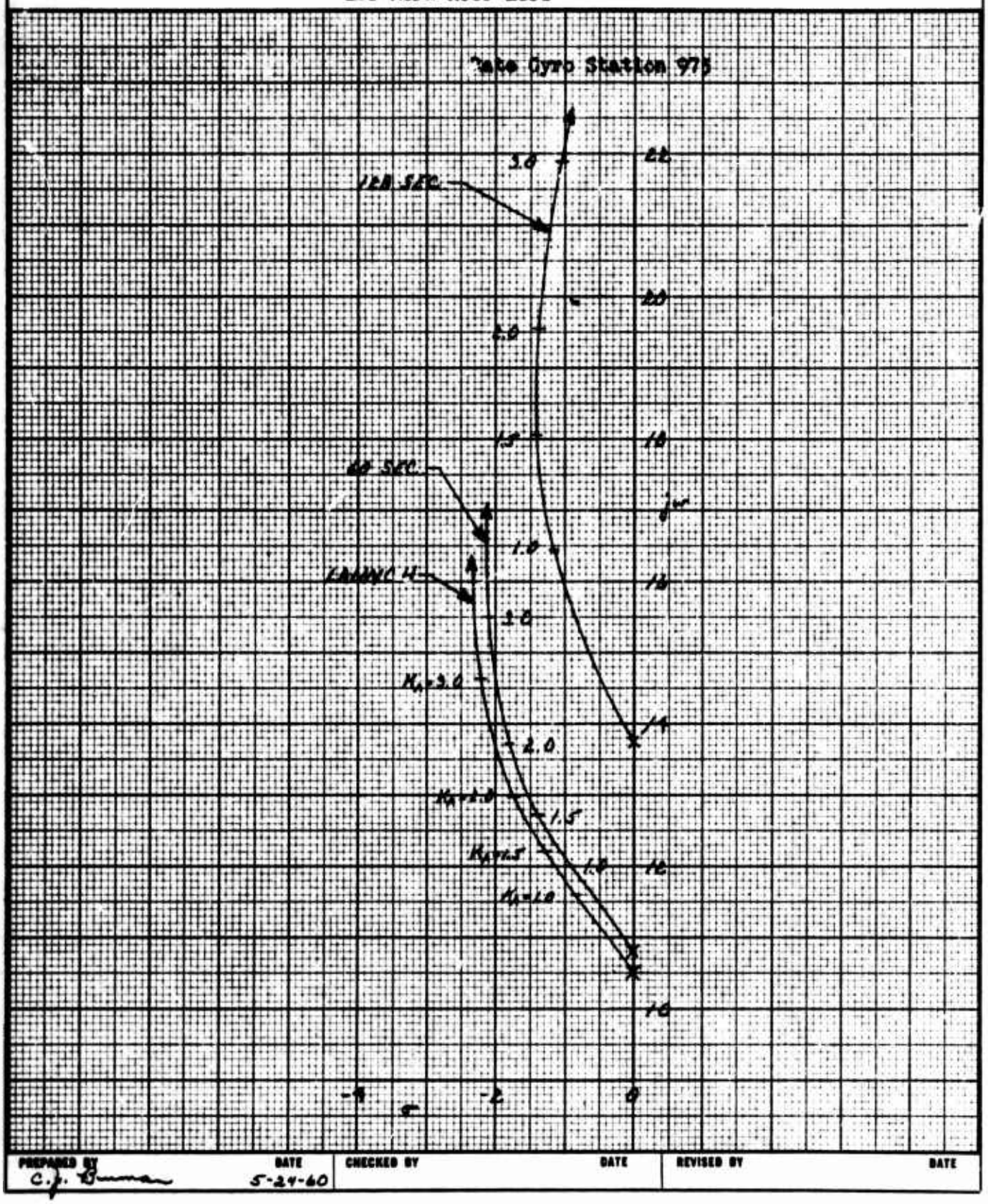

PREPARED BY	DATE	CHECKED BY	DATE	REVISED BY	DATE
C. J. Burman	5-24-60				

FORM NO. A707-1

FIGURE
2ND MODE RO

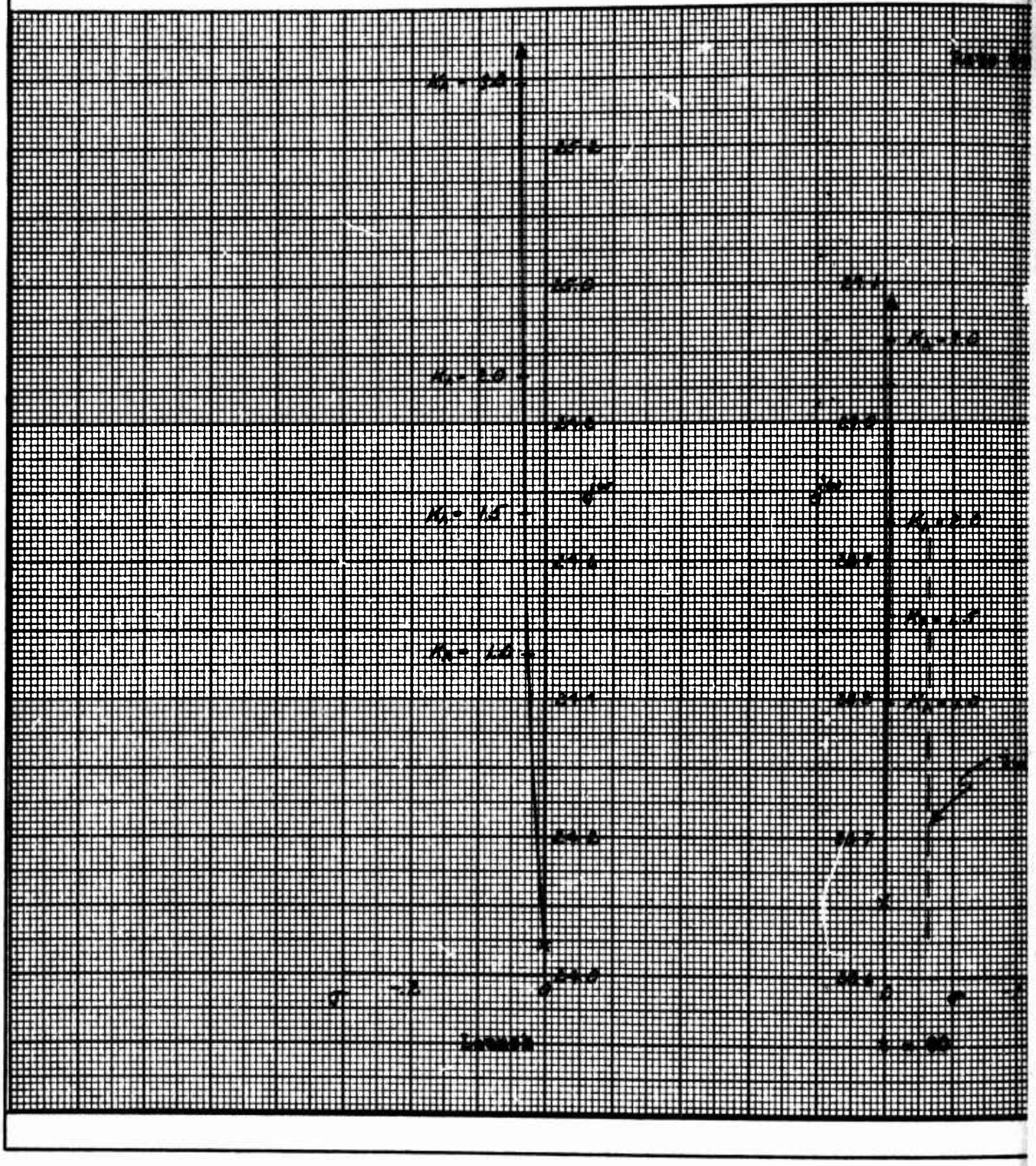

GURE 6.7
DE ROOT LOCI

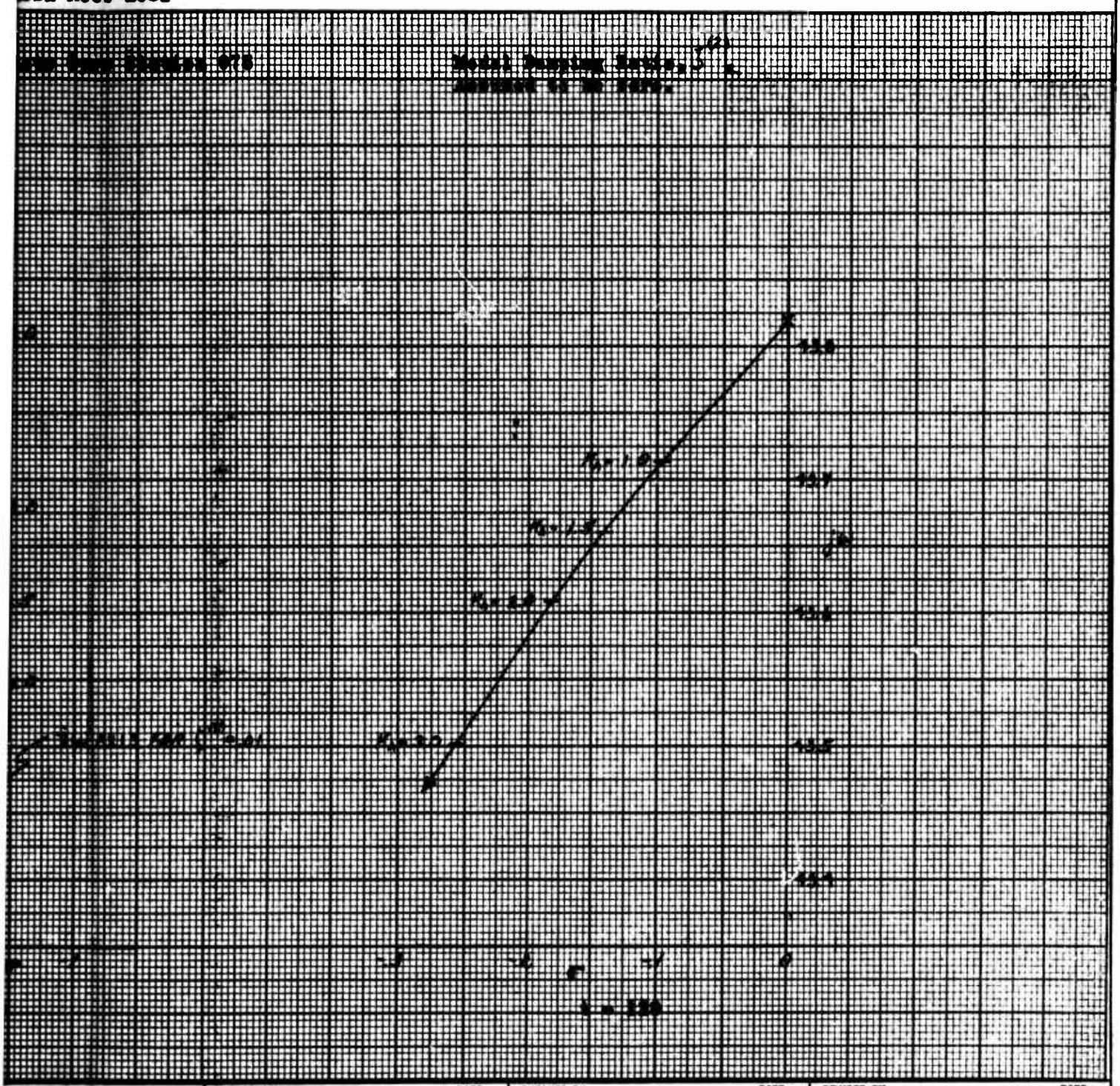

PREPARED BY	DATE	CHECKED BY	DATE	REVISED BY	DATE
C. J. Tuman	5-24-60				

B

CONVAIR ASTRONAUTICS

SECR

FIGURE (
3RD MODE RO(

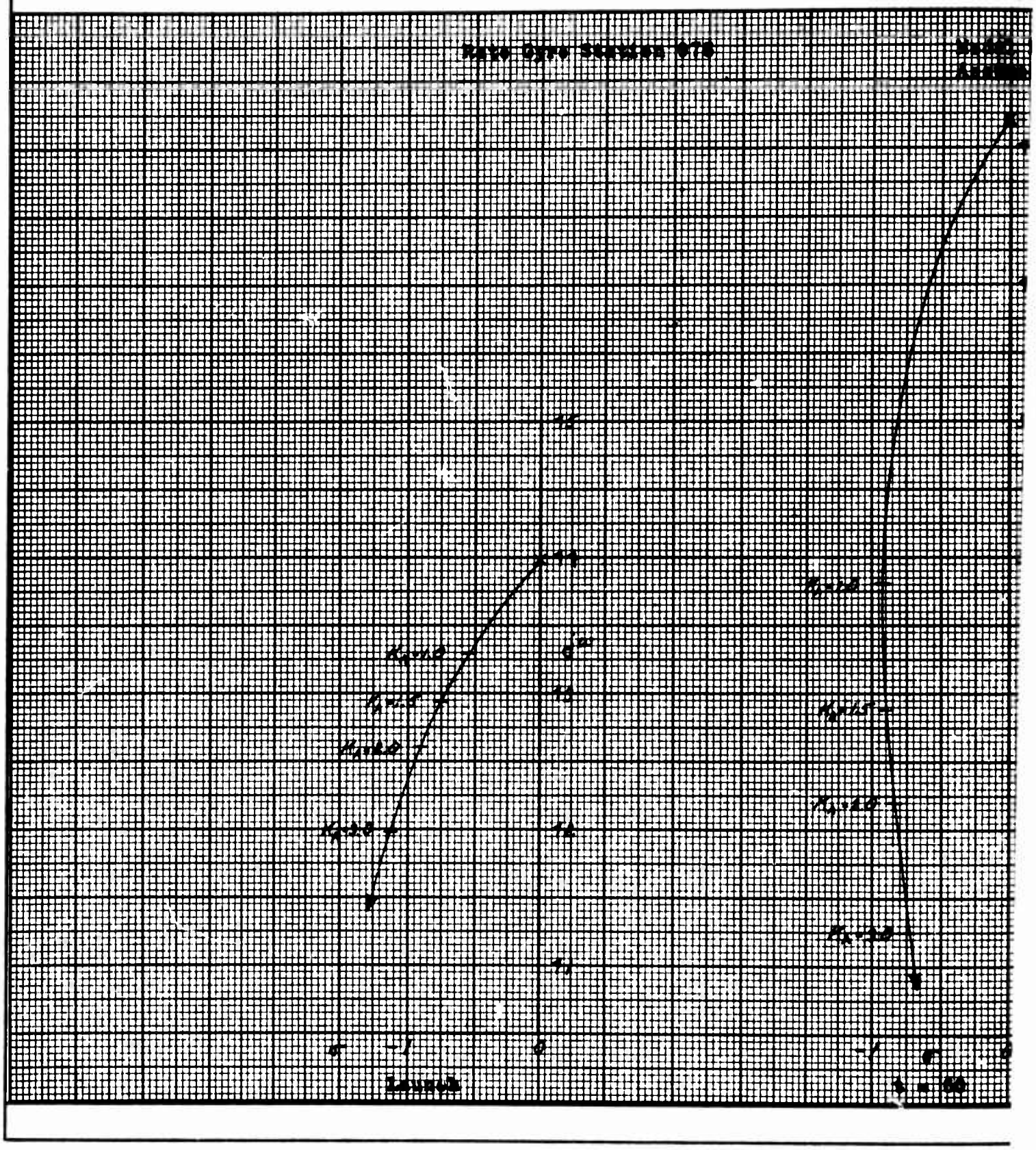

A

FORM NO. A707-2

SEC

FIGURE 5.6
MODE ROOT LOCI

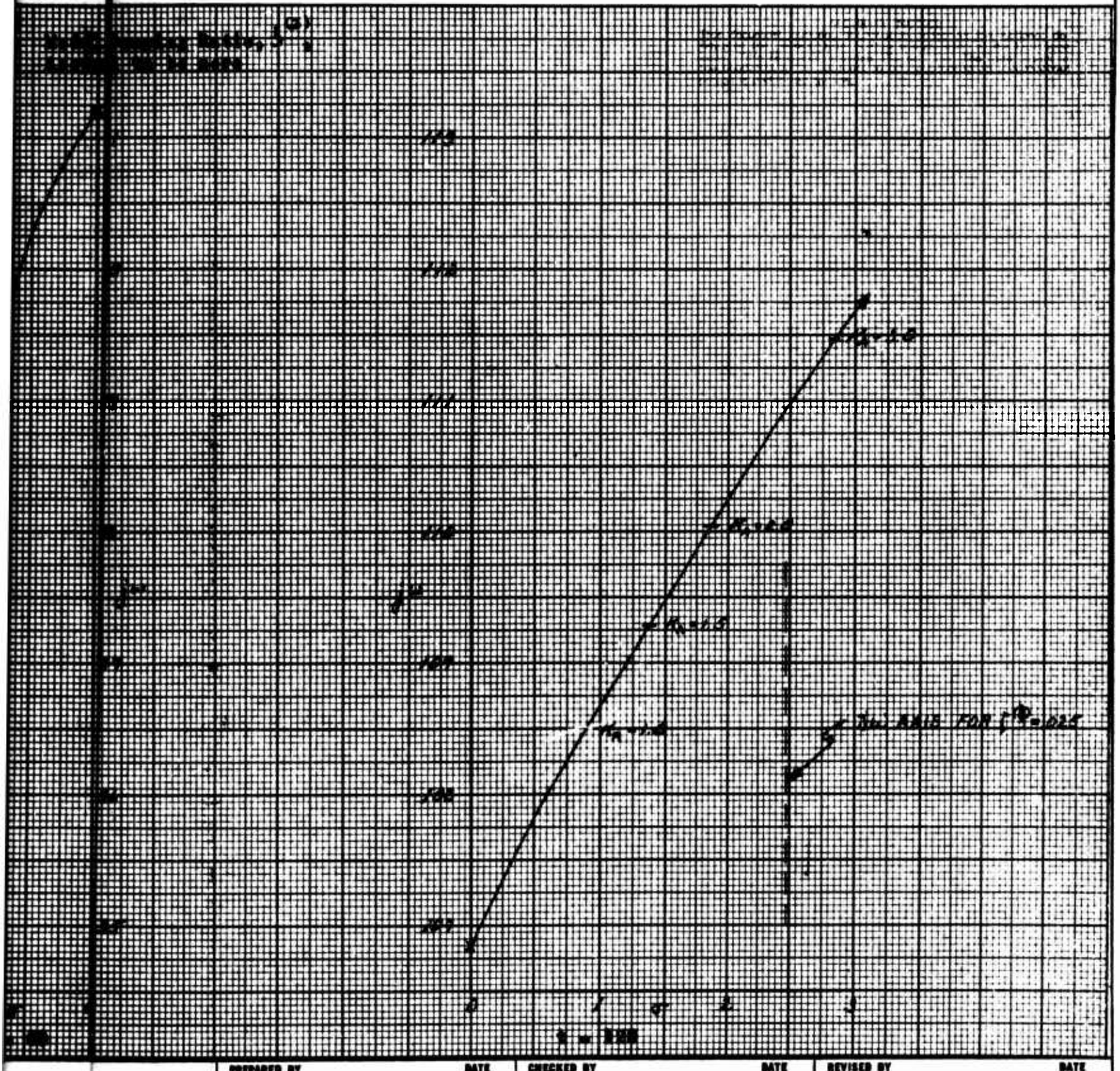

PREPARED BY	DATE	CHECKED BY	DATE	REVISED BY	DATE
C. J. Berman	5-25-60				

B

general understanding can be obtained from a consideration of the locus departure angles from the system poles and of how this angle is influenced by other poles and zeros of the system transfer function. The poles and zeros may be divided into two groups, those associated with the autopilot - the actuator, rate gyro and rate gain, and possibly filters - which are usually fixed during flight, and those associated with the bending modes - the TWD ("tail wags dog") zeros, and the bending dipoles, which can vary during flight as the bending parameters change. These bending poles and zeros can be approximated for the purpose of illustration by

TWD	BENDING DIPOLES
$s^2 + \frac{T_c}{\lambda_R M_R - \frac{I_R \sigma_{XT}}{57.3}}$	$s^2 + \frac{W_i^2}{1 - \frac{I_{RG} \sigma_{(i)}}{57.3 \lambda_c M_i}}$

Although the TWD zero locations vary some, they may be considered fixed since they usually vary over a very small range on the jw axis.

As the mass of the missile decreases during flight the bending frequency, W_i, increases and the bending pole (considering only the positive portion of the axis) moves up to the jw axis. The departure angle from the bending pole can be determined easily by measuring the angles from the other zeros and poles. A 180 degree phase shift occurs whenever the pole passes up through the TWD zero.

Since the quantity $\frac{I\sigma_{RG}^{(1)}}{57.3\ lcMi}$ does not normally have an amplitude greater than about two, a change in the sign of the modal slope $\sigma_{RG}^{(1)}$, (due to an antinode passing through the rate gyro location) causes the bending zero to pass over the bending pole producing 180 degree shift in phase of the departure angle. The bending zero is about the pole when $\sigma_{RG}^{(1)}$ is positive and below the pole when it is negative. For the case of separate rate and position gyro locations the bending zero is not exactly on the $j\omega$ axis but will still produce a rotation of the departure locus that approaches 180 degrees.

The effect of poles or zeros not on the $j\omega$ axis is also used in estimating the rotation of the departure locus. The actuator, for instance, occurs as a quadratic conjugate pair of poles plus a first order lag. Since the bending pole is on the $j\omega$ axis, knowledge of the phase characteristics of first and second order functions can be used to estimate how rapidly the locus rotates.

6.5 Analysis of the Results

No modal damping was included in the equations from which the bending mode loci were calculated. As a result these loci may appear to yield unstable roots (in the Right Half Plane) when such is not actually the case. Actual structural damping measurements obtained as a result of full scale Atlas tests at ERB show that the damping ratios for the first two modes on the Atlas are

as high or higher than the following:

Time	1st Mode	2nd Mode
Launch	.005	.005
60 seconds	.005	.015
128 seconds	.025	.05

The effect of structural damping can be visualized on the root locus plots by shifting the $j\omega$ axis to the right by the amount of the damping ratio multiplied by the frequency of interest ($g^{(i)} X \omega$ without moving the locus. On loci which depart into the RHP plane, a dashed line is drawn to shown the location of the imaginary axis for a conservative value of damping.

6.5 First Mode

The first bending mode, as shown in the root loci of Figure 6.6 is stable at all times since its frequency, ω_1, and slope $\sigma_{RG}^{(1)}$, at the rate gyro location vary little during flight. At launch the first bending mode frequency and the frequency of the LO_2 in the Centaur are very close to the same. The root locus of Figure 6.9 includes the effect of coupling of the first bending mode into the Centaur LO_2 sloshing equation. The fact that no instability arises is shown by the root locus.

6.6 Second Mode

Both at launch and at sixty seconds the second mode locus, shown in Figure6.7, departs at about 90 degrees since there is little change in frequency. The 60 seconds locus is slightly less than 90 degrees and appears to be in the right half plane (RHP). However, including the effect of modal damping, the roots would lie in the left half plane (LHP), as can be seen from the location of the $j\omega$ axis for a conservative value of structural damping ratio, $\zeta^{(2)}$ (as shown on Figure 6.7). As the second mode frequency increases, this locus would rotate slowly clockwise, When the second mode frequency reaches 32 radians, however, the locus departure angle changes by 180 degrees as the modal pole passes over the TWD zero at that frequency. The locus then would be departing toward the LHP. Further increase in frequency results in more clockwise rotation and increased stability. Thus, the

FIGURE 6.9

ROOT LOCI PROPELLANT SLOSHING 1ST BENDING MODE AND CENTAUR LO_2 TANK SLOSHING

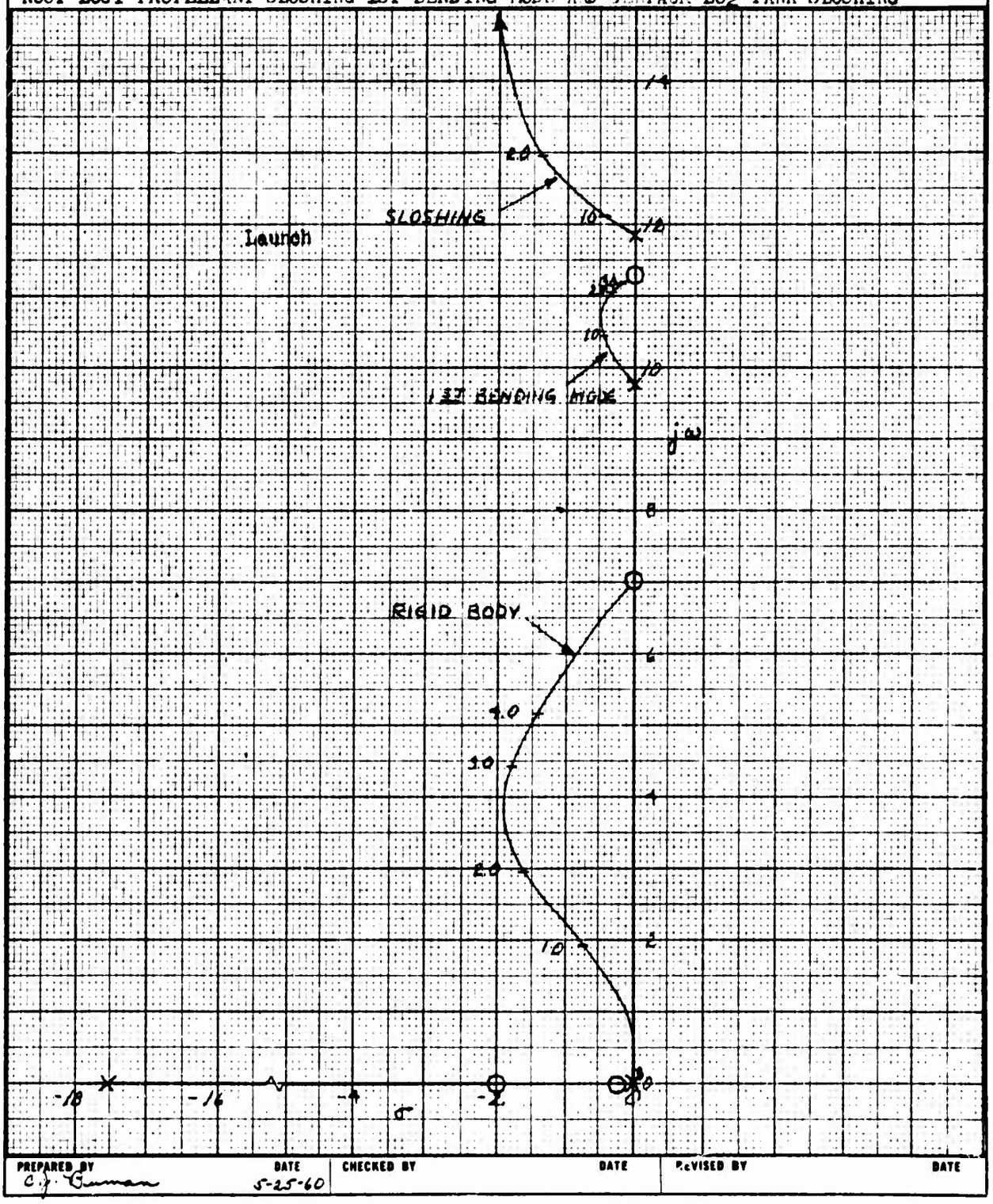

PREPARED BY	DATE	CHECKED BY	DATE	REVISED BY	DATE
C. J. Guman	5-25-60				

second mode is stable at all times.

6.7 Third Mode

The behavior of the loci of the first and second modes is almost exactly the same as for the Atlas F alone. However, the thrid mode, which is phase stable at all times for the Atlas F without Centaur, departs toward the RHP at 128 seconds for the Atlas plus Centaur. The difference arises from the fact that on the Atlas F, the slope, $\sigma_{RG}^{(3)}$, changes sign resulting in the movement of the third mode zero from below (in frequency) the third mode pole to above the pole. This shift in the mode zero, produces a 180 degrees shift in the locus departure angle from the pole just as the departure angle rotates through the 90 degree position and prevents the locus from moving toward the RHP. On the Atlas F plus Centaur, the modal slope does not change sign and the locus continues to rotate clockwise toward the RHP. Consideration of modal damping on Figure 6.8 shows that the third mode is stable for the operating gain ($K_A > 1$). Further gain margine would be obtained by moving the rate gyro package slightly aft.

Since the modal frequencies are low at launch, an analysis of the 4th and 5th having modal frequencies of 58.9 and 73.1 radian, respectively, was made. This analysis revealed that the respective locus departure angles from the fourth and fifth mode poles was 154 and 156 degrees, showing that both modes are phase stabilized.

With increasing flight time these frequencies also increase and provide additional gain stabilization through attenuation by the control system.

Inspection of the mode shapes and frequencies included in the dynamic loads section reveals that the mode characteristics that affect the analysis of the coupling of the autopilot and bending modes for the Atlas F plus Centaur with either the 4000 or 17000 pound payload are almost the same. Due to this similarity, only one payload configuration was analyzed.

6.8 Stability of Sloshing Propellants

The equations used in the analysis of the stability of the sloshing propellants employ a mechanical pendulum analog to represent the sloshing propellants (see References B, C, and D for development of these equations). The system equations at 60, 90, and 120 seconds for three pendulums were solved on the digital computer and the resulting root loci are shown in Figures 6.10 and 6.11 Figure 6.10 represents the Atlas tank sloshing loci and the higher frequency Centaur LO_2 tank at 60 seconds. However, as can be calculated from the location of the Atlas LO_2 sloshing root at the operating gain ($K_A = 1$) this root has a negative (divergent) "damping ratio" of about 0.001. The calculated ratio of slosh angle to engine angle is 120:1 at this time. Since there is only this slight amount of coupling back to the missile and the

FIGURE 6.10
PROPELLANT SLOSHING ROOT LOCI ATL

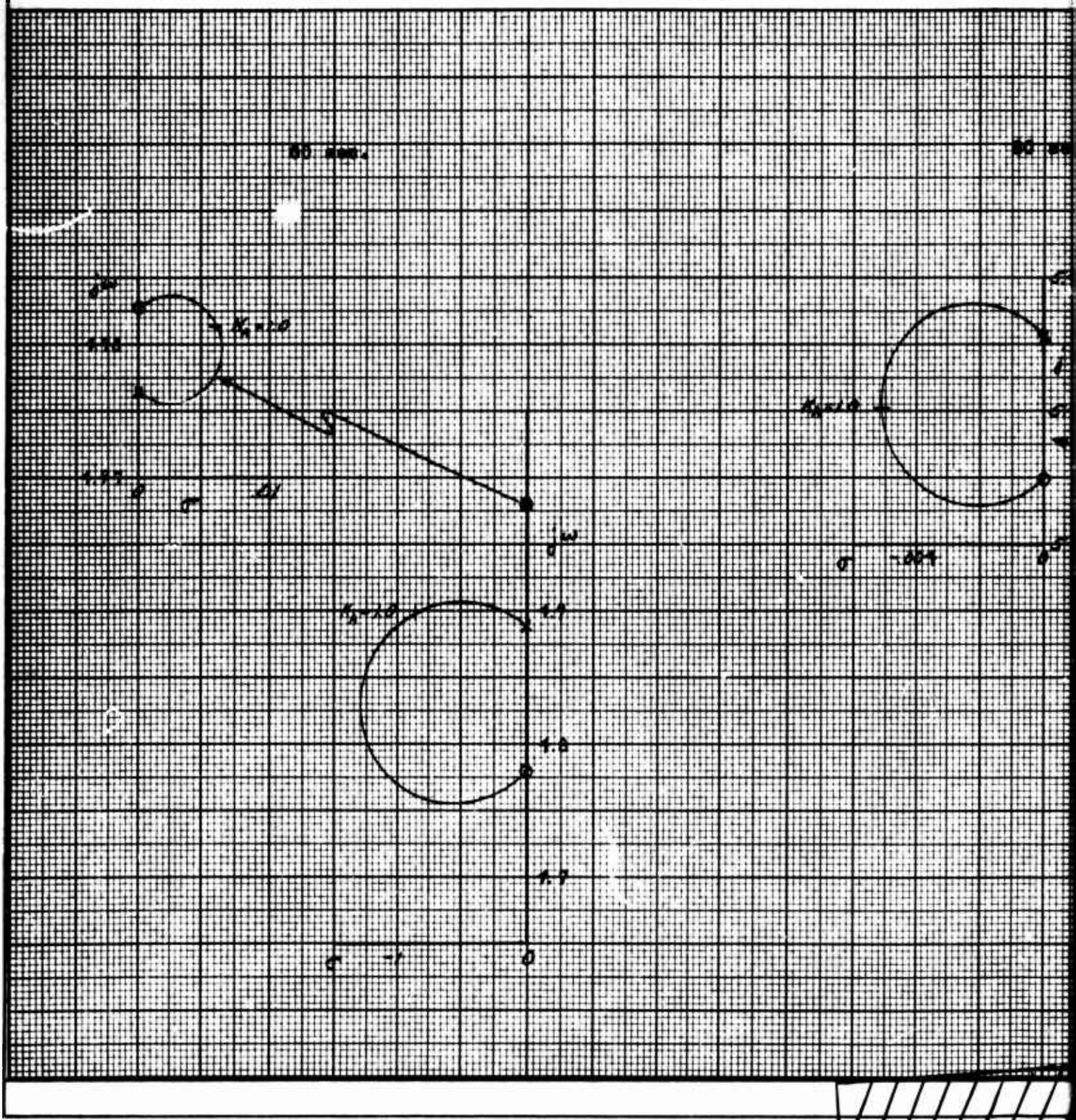

A

URE 6.10
T LOCI ATLAS RPI & LO_2 TANKS

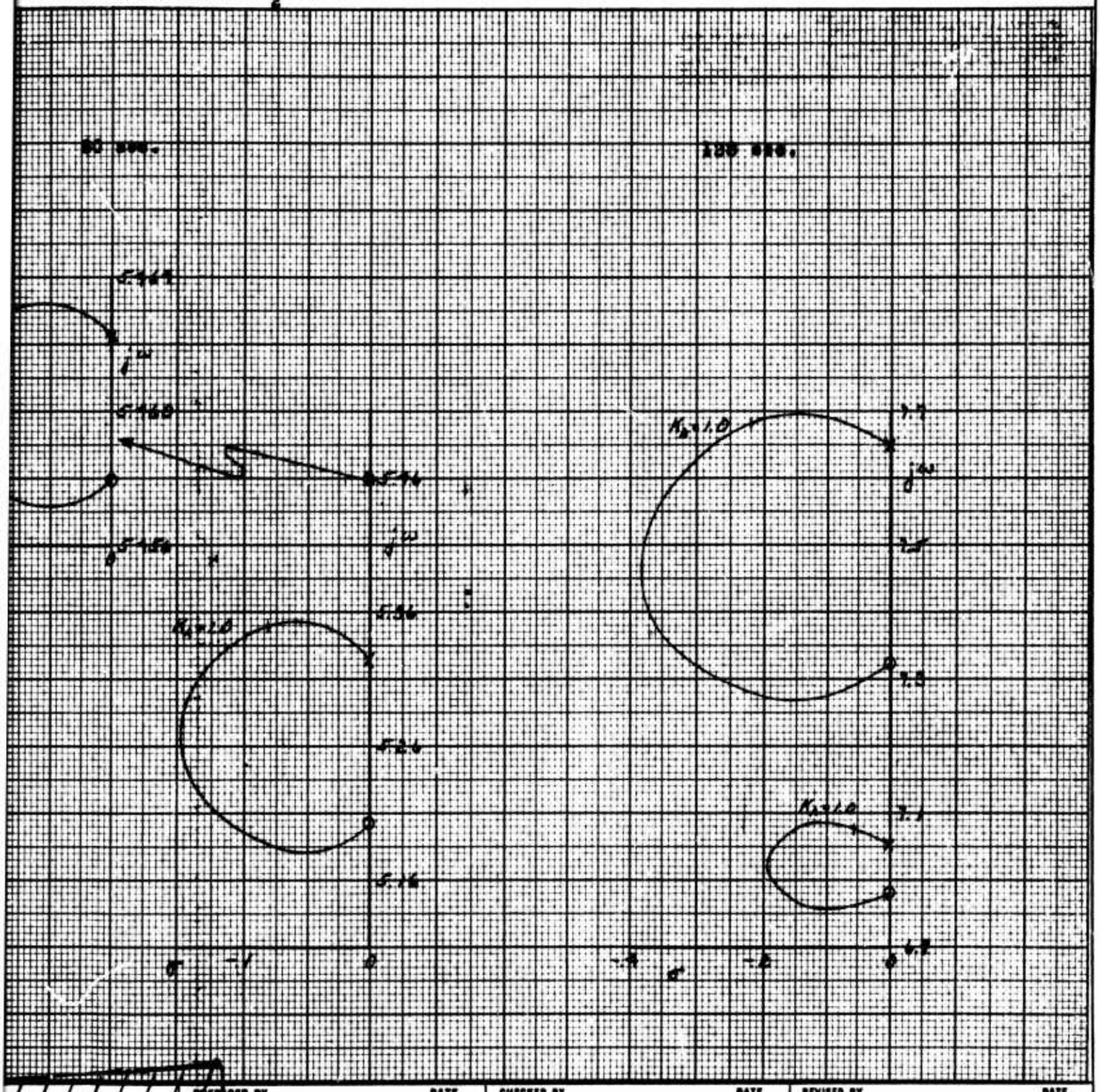

PREPARED BY	DATE	CHECKED BY	DATE	REVISED BY	DATE
C. Luman	5-25-60				

B

1

FIGURE 6.11
ROOT LOCI-CENTAUR LO_2 TANK SLOSHING

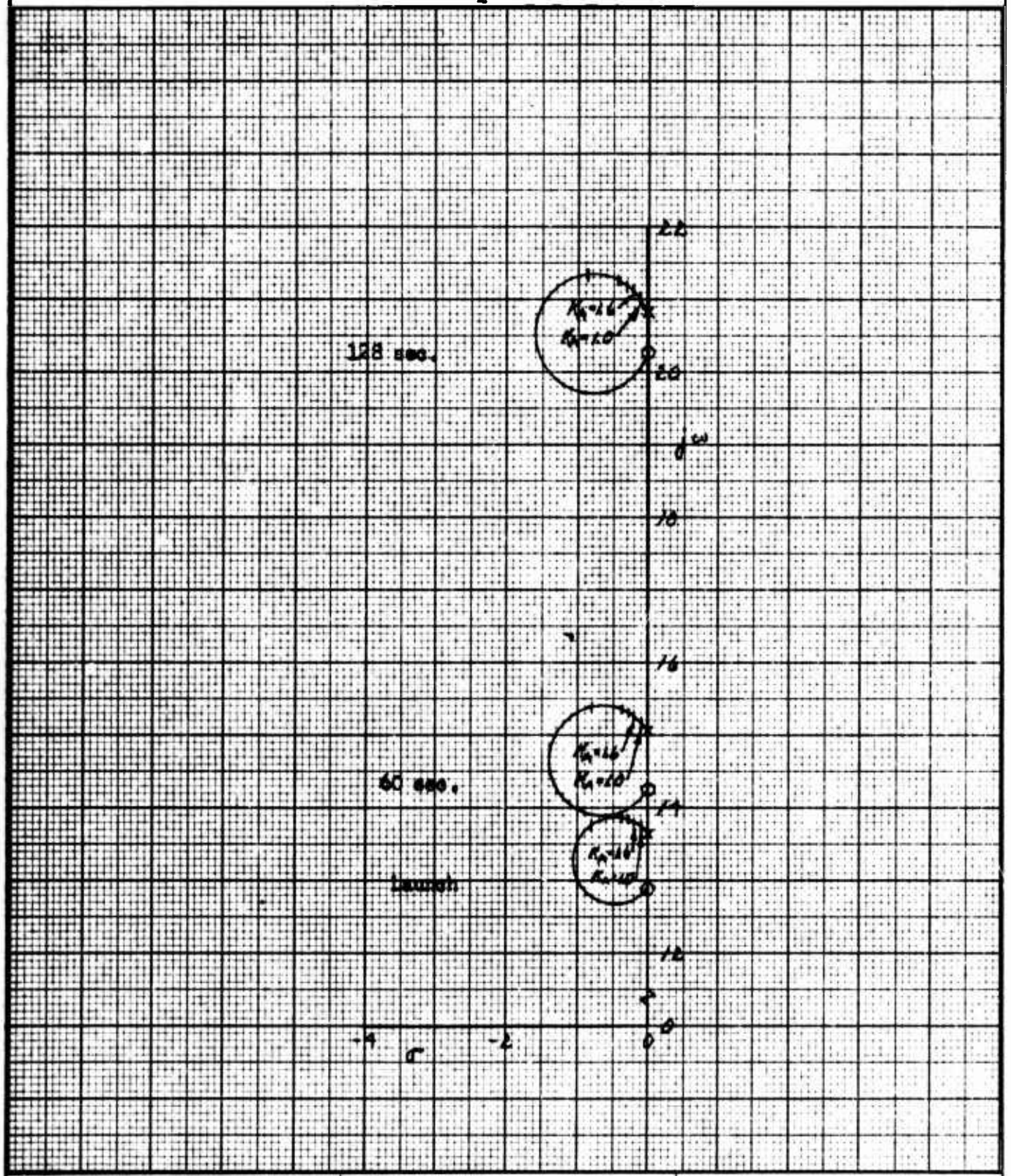

PREPARED BY C.J. Burman DATE 5-25-60 | CHECKED BY DATE | REVISED BY DATE

FORM NO. A707-1

divergent damping ratio is small with instability occurring only for a short time; the number of baffles in the Atlas LO_2 tank can be significantly reduced.

7.0 REFERENCES

A. Convair Report ZU-7-045, "General Theory and Analysis for a Flexible Bodied Missile with Autopilot Control", K. Kachigan 11, November 1955.

B. Convair Report ZU-7-045, "Forced Oscillations of a Fluid in a Cylindrical Tank", K. Kachigan, 4 October 1955.

C. Convair Report ZU-7-069, "Forced Oscillations of Fluid in a Cylindrical Tank Undergoing Both Translation and Rotation", A. F. Schmitt, 10 October 1956.

D. Convair Report ZU-7-074, "Forced Oscillations of a Fluid in a Cylindrical Tank Oscillating in a Carried Acceleration Field-A Correction", A. F. Schmitt, 4 February 1957.